Printing Flexible and Hybrid Electronics for Human Skin and Eye-Interfaced Health Monitoring Systems

Kyunghun Kim, Bongjoong Kim, and Chi Hwan Lee*

Advances in printing materials and techniques for flexible and hybrid electronics in the domain of connected healthcare have enabled rapid development of innovative body-interfaced health monitoring systems at a tremendous pace. Thin, flexible, and stretchable biosensors that are printed on a biocompatible soft substrate provide the ability to noninvasively and unobtrusively integrate with the human body for continuous monitoring and early detection of diseases and other conditions affecting health and well being. Hybrid integration of such biosensors with extremely well-established silicon-based microcircuit chips offers a viable route for in-sensor data processing and wireless transmission in many medical and clinical settings. Here, a set of advanced and hybrid printing techniques is summarized, covering diverse aspects ranging from active electronic materials to process capability, for their use in human skin and eye-interfaced health monitoring systems with different levels of complexity. Essential components of the devices, including constituent biomaterials, structural layouts, assembly methods, and power and data processing configurations, are outlined and discussed in a categorized manner tailored to specific clinical needs. Perspectives on the benefits and challenges of these systems in basic and applied biomedical research are presented and discussed.

1. Introduction

Wearable technology is dramatically growing worldwide in various form factors ranging from wristwatches to fitness bands and to bandage-like patches, which is fueled by continuous improvement of internet of things (IoT), smartphones,

and mobile data connections.[1–4] Given rapidly increased healthcare expenditure and population aging of recent decades, a dominating market segment in wearable technology includes smart healthcare gadgets that offer convenience of access and control in the management of daily health and activity.[5] Wearable monitoring devices provide capabilities for scheduled and continuous evaluation of vital signs and activity (e.g., temperature, blood pressure, perspiration rate, muscle fatigue, and electrophysiological signals) and clinically important biomarkers (e.g., electrolytes, metabolites, and enzymes), which are particularly beneficial to in-home care, rehabilitation, and pain management services to patients with known and suspected health risks.[6–12] The most compelling versions of wearable monitoring often demand direct integration of flexible and even stretchable devices with the human body, allowing for accurate detection and quantitation of the body signals.[2,13–17] The basic requirements for such devices include: i) medical-grade biocompatibility for safety in clinical use, ii) minimal irritation on the body for comfort, iii) easy and unobtrusive fit to a specific area of the body for enhanced usability and improved signal quality (e.g., signal-to-noise ratio), and iv) mechanical longevity and durability throughout the entire lifetime that may involve thousands of cycles of elastic deformations by the body movements. Hybrid assembly of the flexible and stretchable devices with miniaturized silicon-based rigid microcircuit chips provides consumer-grade performance and reliability in data processing and remote transmission, allowing for efficient communications between patients, clinicians, and caregivers.[14,15,17–19]

Concurrently, rapid innovations in advanced materials and hybrid printing technologies have enabled cost-effective and large-batch production of the flexible and wearable electronics,[20–29] offering opportunities to drive widespread deployment of the body-interfaced biomedical monitoring systems to many peoples in need, including those living in rural areas. The basic principles of several printing protocols discussed in this review involve assembling conductive inks and electronic components to a substrate in compact geometries, all under conditions that are compatible with flexible and hybrid printed electronics.[26,28,30–32] The printing protocols enable deterministic assembly of diverse building blocks among the highest performance materials on a flexible and biocompatible substrate with

Dr. K. Kim
Weldon School of Biomedical Engineering
Purdue University
West Lafayette, IN 47907, USA

B. Kim
School of Mechanical Engineering
Purdue University
West Lafayette, IN 47907, USA

Prof. C. H. Lee
Weldon School of Biomedical Engineering
School of Mechanical Engineering
Department of Speech
Language, and Hearing Sciences
Purdue University
West Lafayette, IN 47907, USA
E-mail: lee2270@purdue.edu

The ORCID identification number(s) for the author(s) of this article can be found under https://doi.org/10.1002/adma.201902051.

**ADVANCED
SCIENCE NEWS**

www.advancedsciencenews.com

**ADVANCED
MATERIALS**

www.advmat.de

specific geometries and shapes tailored for a body part.[32–36] Representative examples of the human skin and eye-interfaced health monitoring systems discussed throughout this article illustrate hybrid integration of several printing materials and techniques and show how they are formulated and implemented.

Herein, we first review advanced printing materials and techniques, organized according to the working principles, which have been demonstrated at the consumer level of commercial availability and viability for the past decade. An overview of the general printing protocols and examples of flexible and hybrid printed electronics are described. In the following section, we review several system-level applications of the most promising devices in disease-specific healthcare utilizations, categorized into skin-mountable, eye-mountable and tissue-injectable monitoring and care. The basic materials, device layouts, monitoring schemes, data processing, and transmission configurations, and their clinical implications are also discussed. A graphical summary of these examples appears in **Figure 1**. Overall, we outline all the key components in the human skin and eye-interfaced health monitoring systems and discuss the needs and opportunities to expand the scope of care for patients, along with the difficulties and challenges that remain to be overcome.

2. Advanced Printing Materials and Techniques

Flexible and hybrid printed electronics have attracted a great deal of attention in the past decade, particularly for the production of diverse body-interfaced health monitoring systems in low-cost and large-scale. Different forms of flexible materials and printing techniques have been utilized by relying on a set of parallel protocols to print conductive and dielectric materials and miniaturized electronic microchips for their rational integration into functional and flexible structures with prescribed geometries and configurations. The following sections highlight several widely used printing materials and techniques for flexible or, particularly, wearable applications by categorizing into: i) advanced transfer printing methods and ii) hybrid 3D printing methods. **Table 1** presents a summarized overview of these methods in terms of the working principles, printable materials, and key advantages and challenges.

### 2.1. Advanced Transfer Printing Methods

Traditionally, microelectronics and sensors have been fabricated by using standard semiconductor lithography techniques that typically involve the use of photosensitive polymers, which are extremely well suited to the tasks to define complex microscale patterns on a rigid, flat wafer. However, significant challenges exist in adopting these techniques directly for mechanically flexible and nonflat substrates that are particularly made of biocompatible soft elastomers, mainly due to the required chemical and thermal treatments causing potential damages to the substrates. To circumvent this problem, various forms of transfer printing approaches have been established.[37–46] In general, these approaches represent

Kyunghun Kim received his B.S. (2012) in information display from the Kyung Hee University and his Ph.D. (2017) in chemical engineering from the Pohang University of Science and Technology (POSTECH) in South Korea. He is currently a postdoctoral research fellow of the Weldon School of Biomedical Engineering at Purdue University, working in the Chi Hwan research group. His research focuses on the development of eye-mountable biosensors for diagnosis and management of ocular diseases.

Bongjoong Kim received his B.S. (2012) in mechanical engineering and M.S. (2014) in automotive engineering from the Hanyang University in South Korea. He is currently a Ph.D. candidate of the School of Mechanical Engineering at Purdue University, working in the Chi Hwan research group. His graduate work focuses on the development of advanced transfer printing techniques for construction of 3D electronics and biosensors.
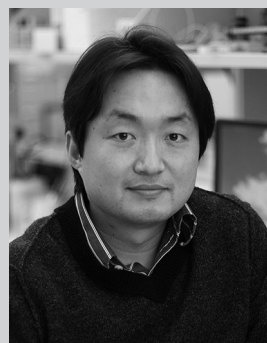
Chi Hwan Lee obtained a B.S. (2005) in mechanical engineering from the Illinois Institute of Technology in Chicago. From Stanford University, he received his M.S. (2007) and Ph.D. (2013) in mechanical engineering. He is currently an assistant professor of the School of Biomedical Engineering, Mechanical Engineering, and the Department of Speech, Language, and Hearing Sciences (courtesy) at Purdue University. His research focuses on the development of body-interfaced bioelectronics and biosensors tailored for specific clinical needs. He is a cofounder and CTO of the Curasis, LLC, and serves as a scientific advisor in Omniply Tech.

a set of techniques that enable the deterministic integration of various classes of materials with a foreign receiver substrate in a large-scale and defect-free manner. These approaches offer remarkable opportunities to construct high-performance electronics and sensors on diverse wearable
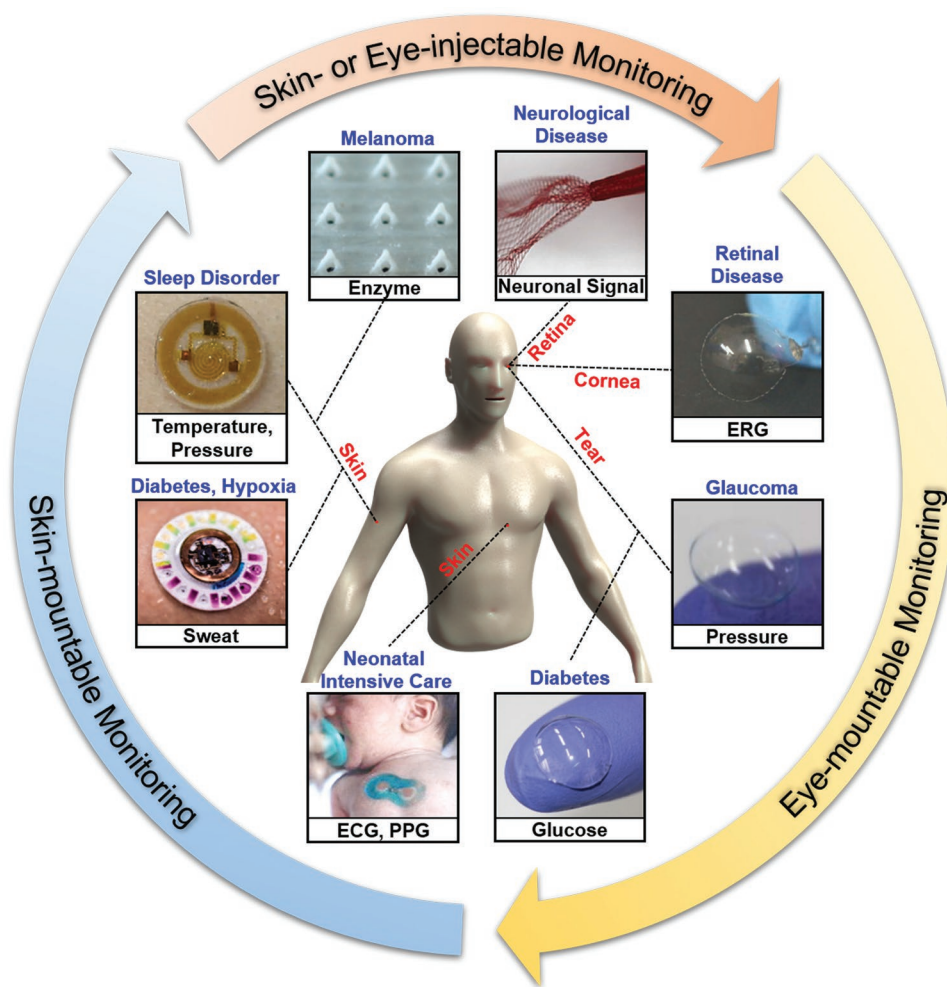
Figure 1. Schematic diagram of the human skin and eye-interfaced health monitoring systems tailored for specific clinical needs. Image for "Neonatal Intensive Care": Reproduced with permission.[17] Copyright 2019, American Association for the Advancement of Science. Image for "Diabetes, Hypoxia": Reproduced with permission.[14] Copyright 2019, American Association for the Advancement of Science. Reprinted/adapted from *Science Advances* **2019**, *5*, eaav3294 © 2019, The Authors, some rights reserved; exclusive licensee American Association for the Advancement of Science. Distributed under a Creative Commons Attribution NonCommercial License 4.0 (CC BY-NC) http://creativecommons.org/licenses/by-nc/4.0/. Image for "Sleep Disorder": Reproduced with permission.[15] Copyright 2018, American Association for the Advancement of Science. Image for "Diabetes": Adapted with permission.[31] Copyright 2018, The Authors, published by American Association for the Advancement of Science. Reprinted/adapted from *Science Advances* **2018**, *4*, eaap9841 © 2018, The Authors, some rights reserved; exclusive licensee American Association for the Advancement of Science. Distributed under a Creative Commons Attribution NonCommercial License 4.0 (CC BY-NC) http://creativecommons.org/licenses/by-nc/4.0/. Image for "Glaucoma": Adapted under the terms of the CC-BY Creative Commons Attribution 4.0 International License (http://creativecommons.org/licenses/by/4.0/).[30] Copyright 2017, The Authors, published by Springer Nature. Image for "Retinal Disease": Reproduced under the terms of the CC-BY Creative Commons Attribution 4.0 International License (http://creativecommons.org/licenses/by/4.0/).[162] Copyright 2018, The Authors, published by Springer Nature. Image for "Melanoma": Reproduced with permission.[210] Copyright 2018, Wiley-VCH. Image for "Neurological Disease": Reproduced with permission.[211] Copyright 2018, American Chemical Society.

substrates in a spatially controlled manner that produces the most complex and sophisticated configurations. **Figure 2** summarizes the most promising transfer printing methods, organized according to their working principles such as: i) sacrificial layer-etching-based transfer printing,[37,47,48] ii) controlled spalling-based transfer printing,[49,50] and iii) interfacial layer delamination-based transfer printing.[39,51,52] These exemplary transfer printing methods discussed in these sections have enabled the realization of custom design services at consumer level for producing diverse microscale electronics and sensors, demonstrating their commercial viability.

2.1.1. Sacrificial Layer Etching-Based Transfer Printing

Figure 2a (left) describes a particularly powerful transfer printing method due to its natural capability to incorporate device-grade monocrystalline semiconducting materials in which the materials are picked up from their growth/fabrication substrates with a soft elastomeric stamp made of polydimethylsiloxane (PDMS) and then printed to a foreign receiver substrate in a parallel manner.[37] The pick-and-place steps occur at room temperature and can be repeated for large-area assembly and/or heterogeneous materials integration in 2D or 3D layouts at

Table 1. A summarized overview of the advanced printing methods in terms of the working principles, printable materials, and key advantages and challenges.

| Printing strategy	Working principles	Printable materials	Key advantages	Challenges	Refs.
Advanced transfer printing	Sacrificial layer etching-based transfer printing	Si/Ge/GaAs/ GaN/InP	Available to various forms of mono-crystalline semiconducting materials	Slow etching process of the sacrificial layer	[37,54–57,59]
				Requirement for postfabrication process on receiver substrates	
	Controlled spalling-driven method	Si/Ge/III–Vs	Transfer of fully fabricated circuits over wafer scale	Requirement for postetching of residual substrate material	[49,50]
				Handling difficulty for the stressed/curved thin films	
	Interfacial layer delamination-based transfer printing	Integrated nanocircuits and sensors	No requirement for postfabrication	Limited in the use of monocrystalline semiconducting materials	[39,52]
			Multiple times reusable donor wafer		
Hybrid 3D printing	Shear-thinning flow behavior	AgNW/AgNP/ Ag flake/ GO/CNT	Printing of uniform/high-aspect ratio motifs	Limited in the printing resolution by nozzle size and ink properties	[26,29,92–95]
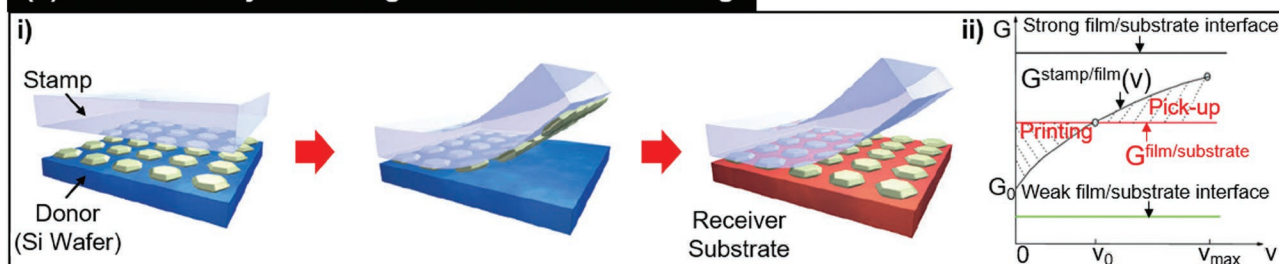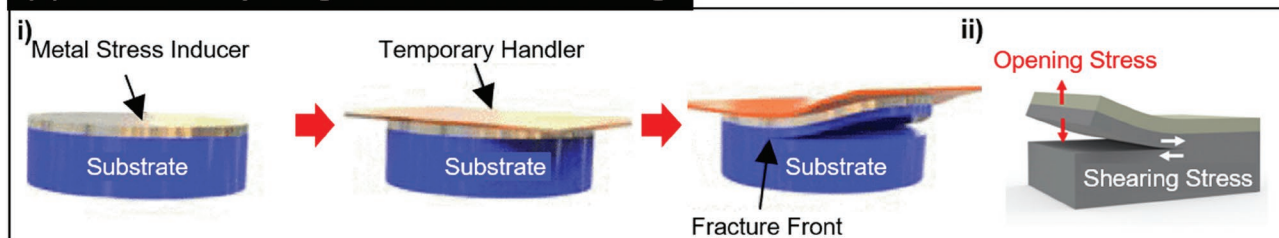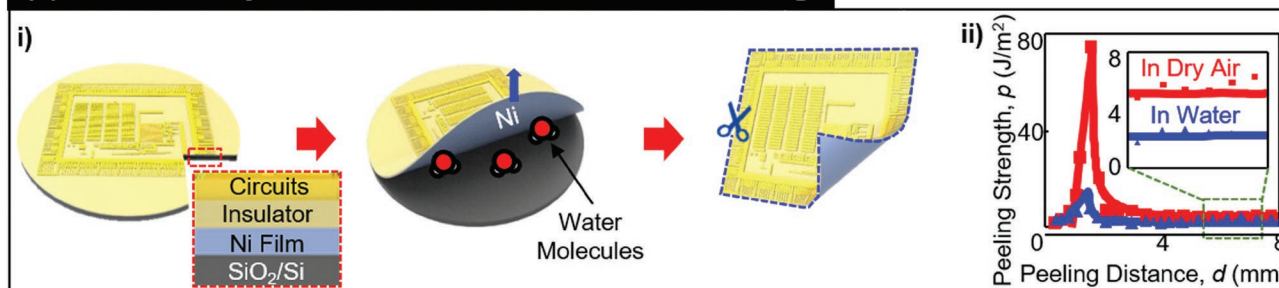
Figure 2. Advanced transfer printing methods. a) Pick-and-place transfer printing method. i) Schematic illustration of the process flow by using an elastomeric stamp. Reproduced with permission.[37] Copyright 2006, Springer Nature. ii) Schematic diagram of critical energy release rates for the film/substrate interface and the stamp/film interface. Reproduced with permission.[47] Copyright 2007, American Chemical Society. b) Controlled spalling-driven transfer printing method. i) Schematic illustration of the process flow by exploiting controlled thermal spalling. Reproduced with permission.[80] Copyright 2016, IEEE. ii) Schematic illustration of the stress field in the spalling fracture mode. Reproduced with permission.[83] Copyright 2014, American Chemical Society. c) Chemomechanics-driven transfer printing method. i) Schematic illustration of the process flow by exploiting controlled interfacial delamination phenomenon. ii) Experimental and finite-element analysis (FEA) results of peeling strength versus peeling distance under wet (water) and dry conditions. c) Reproduced with permission.[39] Copyright 2018, National Academy of Sciences.

microscale by using a micro-XYZ manipulator under microscope examinations. The success of this method relies principally on the competition of the interfacial adhesion and delamination among the printable materials, elastomeric stamp, and donor/receiver substrates, wherein the adhesion between the solid films and the stamp depends on peeling rate (that is, kinetically controllable) due to the intrinsic viscoelasticity property of the elastomeric stamp. Specifically, a rapid peeling ($\geq\approx 10$ cm s^{-1}) of the stamp from the donor wafer leads to the delamination of the materials to the surface of the stamp while a sufficiently slow peeling ($\leq\approx 1$ mm s^{-1}) of the stamp from the receiver substrate allows the materials to remain behind on the surface of the receiver substrate. Transfer printing with various classes of monocrystalline semiconducting materials,[37,53–60] such as Si, Ge, GaAs, GaN, and InP in various forms ranging from 0D dots[61,62] to 1D wires and ribbons,[63–66] to 2D membranes,[57,67,68] and to 3D architectures[69–73] have been successfully demonstrated in this way.

Figure 2a (right) shows a schematic diagram of critical energy release rate (G_{crit}) at the interface of film/substrate ($G^{film/substrate}$) and stamp/film ($G^{stamp/film}$) versus the peeling rate (ν).[47,74,75] To facilitate precise adhesion control of the $G^{film/substrate}$ during the pickup step, additional layer of chemically dissolvable sacrificial film can be inserted in between the semiconducting materials and the donor wafer substrate. An example approach involves the use of multiple stacked semiconductor (i.e., GaAs)/sacrificial (i.e., AlGaAs) films that are epitaxially grown on a host GaAs wafer, followed by immersing in a proper etchant solution (i.e., hydrofluoric acid, HF) to remove the sacrificial layer exclusively, resulting in the physical release of the remaining semiconducting materials.[76] Subsequently, the abovementioned pick-and-place operation can be repeatedly employed to deliver the released semiconducting materials to a receiver substrate in a spatial layout that matches specific requirements for electronics. During the printing step, a pulsed laser beam (power: 30W; wavelength: 805 nm; minimum pulse width: 1 ms) can be also applied to facilitate precise adhesion control of the $G^{stamp/film}$ where the laser beam is focused at the interface while the transparent stamp allows the laser radiation to transmit through.[41] Here, the picked solid materials serve as a heat source to raise the temperature of the stamp by 250–300 °C, yielding thermal expansion and curvature in the stamp and leading to the physical release of the solid materials from the stamp.[77] This laser-assisted approach is to eliminate the need for precise control of the interfacial adhesion between the stamp and the receiver substrate, regardless of the pitch size and density of the printed structures. The subsequent step includes the postfabrication required for defining other necessary conducting, dielectric and encapsulation layers on the receiver substrate to yield the complete functional device. This pick-and-place transfer printing method has provided great achievements over the past decade wherein various classes of electronics and sensors have been successfully realized on a range of flexible, stretchable, and wearable substrates including polyurethane, polyimide, and silicone elastomers.[53,78,79] However, the choice of the receiver substrates remains impeded by which the receiver substrate materials must contain certain degree of thermal and chemical resistance to accommodate the postfabrication conditions. Another challenge exists in the printed structures configured with high pitch or low density,

which may give rise to stamp collapse, specifically when high printing strength is subjected to compensate for misalignments between the stamp and the substrate. This may increase a risk of potential damages to both the donor and receiver substrates.

2.1.2. Controlled Spalling-Based Transfer Printing

Figure 2b (left) shows another notable transfer printing method by exploiting a controlled thermal spalling that occurs underneath and parallel to the top surface of the donor wafer.[80,81] The process begins by fabricating complete electronics on a conventional wafer through standard microfabrication technology without any limitation in the use of chemical and thermal processes. The next step involves depositing a relatively thick metal layer such as Ni (6 µm), Ag (20 µm), and Al (50 µm) on the top surface of the donor wafer by using either sputtering or screen printing to serve as a stress inducer.[81,82] A subsequent rapid annealing of the entire structure at >900 °C for a few seconds in a belt furnace followed by cooling down leads to a large thermal contraction between the stress inducer layer and the donor wafer, yielding stresses underneath the wafer to crack the top layer. As a next, the residual wafer materials and buffer layer are chemically etched (e.g., Ge film removed from hydrogen peroxide, H_2O_2) while the donor wafer is required to be polished for recycle.[50] The basic mechanism of this method relies on the controlled spalling that can be propagated from an edge of the donor wafer all the way through the other end, allowing for wafer-scale processing. The stress field of this controlled spalling is composed of both pure opening stress and the shear stress components at the crack tip where the crack tends to follow the trajectory at which the shear stress can be minimized (Figure 2b, right).[83] The equilibrium depth of the spalling typically appears at the location a few microns below the top surface of the wafer, which is underneath the prefabricated thin film electronics. The spalling depth is determined by adjusting the thickness of the stress inducer layer. The use of this method has generated a wide variety classes of flexible electronics such as thin film integrated circuits,[81,84] photovoltaics,[49,50] and energy harvesters[85] by exploiting various classes of epitaxially grown monocrystalline semiconducting elements including Si, Ge, and III–Vs. Although this method has not been utilized for biomedical applications yet, the wafer-scale integration of monocrystalline semiconducting element-based electronics provides a great potential for its future applications in high-performance flexible thin film bioelectronics and sensors. However, challenges still remain in the requirement of the postetching process to remove residual substrate materials and the additional mechanical polishing step to remove kerfs on donor wafer for recycles. The required special handling for the stressed and curved thin films after the spalling process yields an impediment to be overcome.

2.1.3. Interfacial Layer Delamination-Based Transfer Printing

In the abovementioned transfer printing methods, the donor fabrication wafer is often sacrificed by chemical etching or spalling, and cannot be directly recycled. More recently, interfacial layer delamination-based transfer printing methods are developed

in which thin film electronics can be physically delaminated from the fabrication substrate over wafer-scale under manipulated conditions such as induced chemomechanics reactions at the interface,[39,83,86,87] and precisely controlled weak interfacial adhesion,[88,89] all in a defect-free manner that allows the donor wafer to be reused for next fabrication cycles. This aspect serves as a major cost-saving factor in the manufacturing schemes. Figure 2c (left) schematically describes the entire transfer printing protocols of the most recent demonstration:[39] i) The process begins by fabricating desired thin film electronics on a Si wafer that is coated with a ductile metal film such as Ni (≈300 nm) and diluted polyimide (1:1 mixture of 1-methyl-2-pyrrolidinone and polyimide, ≈300 nm), ii) The next step involves mechanical peeling of the thin-film electronics with a temporary handling holder such as thermally releasable tape (Nitto Denko) in distilled (DI) water at room temperature, which allows the bottom Ni film together with the thin-film electronics to be cleanly delaminated from the Si wafer, iii) The physically peeled thin-film electronics can be then pasted to the surface of an arbitrary substrate or surface such as papers, building windows, and flowerpots, thereby allowing such everyday objects to provide useful electronic capabilities, and iv) Removal of the temporary handling holder from the surface completes the entire process.

The basic underpinned mechanism of the defect-free interfacial debonding is relied on a chemomechanics reaction with water molecules at the debonding tip. Figure 2c (right) shows representative experimental (dots) and computational (lines) results that reveal the relationship between peeling strength (p) versus peeling distance (d). These results indicate that the debonding strength under wet (water) condition is largely decreased comparing to that under dry condition (20% relative humidity), and also confirm that the presence of water indeed reduces the interfacial adhesion and thereby promote the intact debonding. However, this method is limited in the performance of the resulting electronics because the epitaxial growth of monocrystalline semiconductor materials is not allowed due to the bottom Ni film. To overcome this, a hybrid transfer printing approach can be used: i) The first step involves the use of the abovementioned pick-and-place transfer printing method to define homogeneous or heterogeneous combinations of monocrystalline semiconducting materials on desired locations of the D-PI/Ni/Si wafer, followed by standard microfabrication processes to yield the complete electronics, and then ii) the chemomechanics-driven interfacial debonding process is followed to physically separate the prefabricated thin film electronics from the Si wafer and subsequently print onto an arbitrary substrate or surface.

2.2. Hybrid 3D Printing Methods

Recent remarkable advances in 3D printing technologies provide versatility to form functional inks on a substrate in both uniform and high-aspect-ratio motifs at microscale.[28,90] The most common types of 3D printing involve direct writing of conductive and dielectric inks on a three-axis computer-controlled translation stage, enabling for creation of complex architectures and compositions in 3D layouts.[26,28,29,32,91] Various classes of conductive inks are used by exploiting micro/nanoscale materials such as silver nanowires (AgNWs),[92]

silver flake,[26,29,93] carbon nanotube (CNT),[94] and graphene oxide (GO).[95] Complex fluids made of biocompatible, flexible, and even stretchable polymer solutions can be also extruded through the nozzle, enabling many useful biomedical architectures and devices, including biosensors,[26,28,96] cell-seeded matrix,[35] and microphysiological systems.[93] Here, the viscoelasticity of the inks is precisely engineered and tailored to maintain the desired morphologies and shapes during the entire period of printing process while simultaneously allowing the inks to flow through nozzles without clogging. Importantly, the ink fluids exhibit a shear-thinning flow behavior, as described by the Herschel-Bulkley model[97]

$$\tau = \tau_y + K\dot{\gamma}^n$$

where τ is the shear stress, τ_y is yield stress, K is the consistency, $\dot{\gamma}$ is the shear rate, and n is the flow index ($n < 1$ for the shear-thinning fluids). During writing process, the applied stress at the tip of the printing nozzle must exceed the yield and shear stresses of the inks. The general ranges of ink viscosity, minimum nozzle diameter, and printing velocity are 10^2–10^6 mPa s, 1–250 µm and 1–100 mm s^{-1}, respectively.[98] More recently, hybrid 3D printing methods have been emerged for producing flexible and stretchable circuits in which the overall process combines direct writing of conductive and dielectric inks with pick-and-place transfer printing of active electronic components (e.g., silicon-based rigid microcircuit chips such as microcontroller, microprocessor, and Bluetooth module), allowing for highly integrated wireless sensing for the human body-interfaced monitoring applications.[29,96] The computer-aided control of these methods provides sophisticated and inexpensive industrial platforms for producing flexible and hybrid printed circuits, all under ambient environments without the need of any harsh chemical, thermal, and mechanical processing conditions, potentially allowing for its commercial mass customization. The following sections introduce recent notable examples of the printed flexible and hybrid circuits on: i) moving freeform surfaces such as the human skin and ii) wearable substrates (**Figure 3**).

2.2.1. Hybrid 3D Printing on Moving Freeform Surfaces

Figure 3a (left) shows an advanced hybrid 3D printing method that involves the direct writing of functional inks on moving freeform 3D surfaces such as the human skin with closed-loop feedback and computer-vision-based control systems by using a compact (380 mm × 680 mm) and portable (≈7 kg) extrusion-based 3D printer.[96] This method exploits a fast drying conductive ink (≈10 min under ambient condition), allowing it to be directly printed on the human skin for its potential applications in health monitoring. The conductive ink used in this work contains silver flakes (10 µm in diameter, Sigma-Aldrich) filled inside poly(ethylene oxide) (PEO, M_v = 1 000 000 Da), providing high conductance (≈1.38×10^4 S cm^{-1}) and sufficiently large viscosity (≈1000 Pa s). This ink exhibits a typical shear-thinning behavior tailored for controllable extrusion during the writing.

The process begins by acquiring the detailed geometric information of the moving target via a light scanner (HDI 109, LMI Technologies) that is combined with real-time estimation
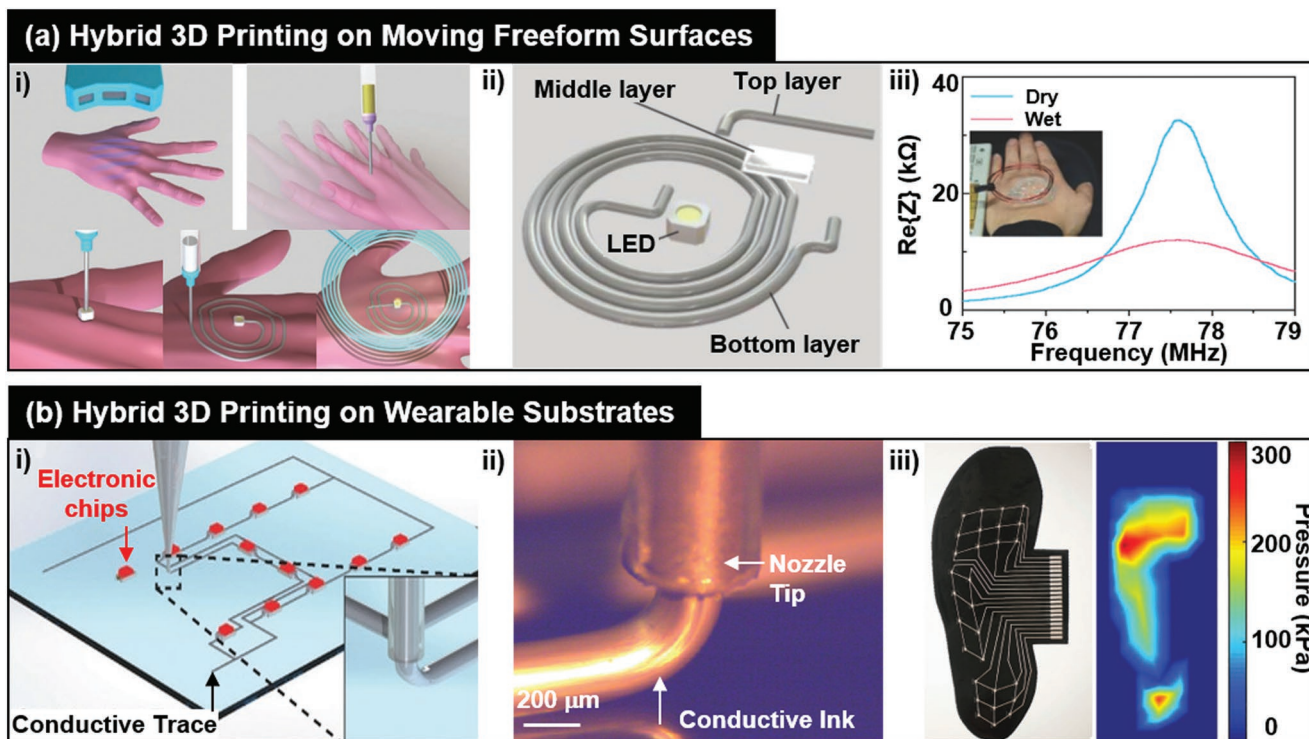
Figure 3. Hybrid 3D printing methods. a) Hybrid 3D printing on moving freeform surfaces. i) Schematic illustration of the process flow for the adaptive 3D printing of multifunctional devices on a moving hand. ii) A 3D printed wireless device comprised of an inductive coil, insulating layer, and conductive traces from the bottom along with a surface-mounted LED, iii) The impedance responses of the device due to the change of moisture level on the surface of the hand. a) Reproduced with permission.[96] Copyright 2018, Wiley-VCH. b) Hybrid 3D printing on wearable substrates. i) Schematic illustration of the process flow that combines direct writing of conductive and dielectric inks and pick-and-place transfer printing of miniaturized rigid electronic chips. ii) Photo of the inks exiting from the nozzle. iii) Photo (left) and IR measurement (right) of the pressure response obtained with the sensor arrays embedded in the insole of a shoe. b) Reproduced with permission.[29] Copyright 2017, Wiley-VCH.

of the motion and then transferred to the motion controller (Chameleon3, FLIR). The next step involves the pick-and-place transfer printing of miniaturized rigid electronic chips to the desired location of the moving target, followed by direct writing of both conductive and dielectric inks in a spatially controlled layout. A demonstrative device constructed in this way includes a wirelessly addressable moisture sensor that seamlessly integrated with the human skin. Specifically, the device is composed of an inductive coil, insulating layer, and conductive traces from the bottom, along with a surface-mounted light emitting diode (LED) to serve as the electrical load of the circuit (Figure 3a, middle). The electrical properties of the circuits can be characterized by adjusting the number of turns for the inductive coils. The printed conductive traces exhibit higher impedance under wet condition comparing to that under dry condition, and any change of the impedance by the moisture level of the skin leads to distinguishable frequency responses of the readout unit (Figure 3a, right).

This printing method can be cost-effective through the automotive robotic system aided by computer vision. A great interest in this context exists in the use of this method for printing extended types of sensors that are capable of recoding electrophysiological and electrochemical biosignals, to serve as the seamlessly skin-mountable diagnostic tools tailored for a specific patient. Further improvements would be necessary to enhance the printing speed ($\approx$7 mm s^{-1}) and the resolution of printable patterns ($\approx$100 µm).

2.2.2. Hybrid 3D Printing on Wearable Substrates

Figure 3b (left) shows another example of the hybrid 3D printing method that combines direct writing of flexible and stretchable inks with pick-and-place transfer printing of miniaturized rigid active electronic chips in a programmable manner.[29] The conductive ink used in this work contains a thermoplastic polyurethane (TPU) and percolating network of silver flakes ($\approx$2 µm lateral dimension) to serve as a biocompatible soft matrix and a conductive filler, respectively. This composition allows the resulting ink to exhibit a strong shear thinning behavior and retain the printed trace width of $\approx$100 µm upon exiting the nozzle (Figure 3b, middle). Whereas the pure TPU (without the silver flake) is a Newtonian fluid with a low apparent viscosity of $\eta \approx 40$ Pa s in which the ink would readily wet and spread on the most of wearable substrates such as textiles. The silver flakes within the TPU can be aligned by shear stress induced during the direct writing process, which gives rise to a conductivity enhancement.[99,100] The conductive ink is not only flexible but also stretchable in which the overall resistance of the printed ink (<4 Ω) is retained under multiple cycles of repeated loading and unloading up to 30% of strain. The conductivity is decreased down to 0.1 S cm^{-1} at the strain of $\approx$200% and then undergoes mechanical and electrical failure at the strain of >240%.

The process begins by writing conductive and dielectric inks on a soft, wearable substrate in a prescribed layout tailored for specific design needs. The next step invovles the pick-and-place transfer printing of active electronic chips in the desired locations of the substrate by exploiting vacuum through an empty nozzle within the positional error of 136 µm ± 62 and the rotational error of 1.45° ± 1.05 ($n = 27$). Here, small droplets of the pure TPU are also printed underneath the printed electronic chips for ensuring their physcial bonding to the substrate. At last, conductive traces are directly printed along a preprogrammed pathway to form the electrical interconnections. System-level demonstrations of this method include the construction of various flexible and hybrid circuits including LEDs and sensors for the detection of strain and pressure. Figure 3b (right) shows an example of the printed circuit system that contains 29 capacitive sensing elements on a soft, flexible substrate that is inserted into the insole of a shoe. The capacitive sensor consists of a dielectric layer using the pure TPU (≈160 µm thick) sandwiched in between the top and bottom electrodes using the silver-flake-mixed TPU (≈40 µm thick). Each of the sensing elements is encapsulated with additional TPU (≈150 µm thick) and placed with a rigid acrylic inclusion on the top where externally applied pressure can be concentrated. The results show that the capacitances of the sensor arrays are reliably responsive to the applied pressures during walking, without suffering from mechanical damages or plastic deformations of the sensors.

This printing method provides a unique route for printing flexible and hybrid circuits in various customized configurations, which would provide many opportunities in personalized wearable devices. In this context, another great interest may exist in the use of this method for printing flexible and hybrid circuits directly on commercial wearable garments such as gloves, socks, and caps, providing ergonomic seamless design for the human body and thereby allowing for comfortable and accurate monitoring of biosignals. Potential improvements would be the employment of broader set of printable materials including ceramics, polymers and metals into this hybrid 3D printing scheme, in order to furthermore expand the functionalities of the printed devices.

3. Clinical Implementation of the Printed Electronics

Early detection of diseases is critically important not only to improve patient health but also to reduce medical expenditure in which, on frequent occasions, the diagnosis based on patients visit to clinics and hospitals with noticeable signs or symptoms is not enough or overly late for discovering many diseases such as cancers, metabolic diseases, and neurodegenerative disorders.[101,102] Therefore, body-interfaced health monitoring systems that allow for accurate and on-demand evaluation of health conditions and symptoms as noninvasively and comfortably as possible would provide important supports in improving the access to early detection, preventive intervention, and pain management.[1,4,11,12,103] Meanwhile, the advances of the abovementioned printing flexible materials and hybrid printing techniques have enabled the advent of many useful noninvasively wearable or minimally invasively injectable biosensors. In this section, we discuss about several current state-of-the-art health monitoring systems in: i) skin-mountable, ii) eye-mountable, and iii) skin- or eye-injectable form factors. **Table 2** presents a summarized overview of these devices in terms of their clinical implementations, biomarkers/biosignals, and key features by comparisons with their conventional clinical methods.

3.1. Skin-Mountable Monitoring Systems

Wearable sensor technology represents major areas of emerging commercial opportunity in noninvasive biomedical research and diagnostics. The most compelling versions of wearable sensors demand direct, seamless contact to the human skin, allowing for reliable recording of vital physiological and electrophysiological biosignals.[104–106] Recent advances in materials engineering, mechanics, and electronics establish the foundation for thin, flexible, and stretchable electronics that can conform to the complex, textured surface of the human skin even under elastic skin deformations.[14,15,17] The following sections introduce several representative examples of

Table 2. A summarized overview of the human skin and eye-interfaced monitoring systems in terms of their clinical implementations, biomarkers/biosignals, and key features by comparisons with their conventional clinical methods.

	Clinical applications	Biomarkers/biosignals	Key features	Conventional clinical methods	Refs.
Skin-mountable	Sweat analysis	Sweat	Miniaturized, wireless, battery-free, noninvasive	Filter paper/gauze pad with benchtop instruments	[14]
	Sleep monitoring	Temperature, pressure		IR imaging system/rectal probes	[15]
	Neonatal intensive care	ECG, PPG		Multiple wires connected to rigid sensors	[17]
Eye-mountable	Retinal disorder diagnostics	ERG	Conformal corneal contact	Corneal/conjunctival electrodes	[162]
	Glaucoma monitoring	Pressure	Wireless, nonInvasive	On-demand measurements	[30]
	Diabetes care	Glucose	Wireless, noninvasive	Finger pricking	[31]
Skin- or eye- injectable	Melanoma screening (skin-injectable)	Enzyme	Wireless	Immunohistochemical staining	[210]
	Neurological disorder monitoring (eye injectable)	Neuronal signals	In vivo recording at the single neuron level	Si/metal/polymer probes	[202]

**ADVANCED
SCIENCE NEWS**

www.advancedsciencenews.com

**ADVANCED
MATERIALS**

www.advmat.de

the skin-mountable health monitoring systems by categorizing them into its clinical implementation in: i) sweat analysis, ii) sleep monitoring, and iii) neonatal intensive care (**Figure 4**). The examples discussed in these sections present the most advanced tools for miniaturized, wireless, battery-free and non-invasive monitoring, which nearly reach at consumer level.

3.1.1. Sweat Analysis

Among various biomarkers such as blood, interstitial fluid, tear, urine, saliva, and sweat to serve as a physiological indicator of human's health conditions, sweat is an ideal candidate because it can be noninvasively collected on the skin at convenient locations of the body.[103] Sweat contains a wealth of chemical information that can potentially indicate the body's deeper biomolecular state.[103] For example, sweat lactate serves as a mean to provide the information of physical stress and thereby can identify transitions from aerobic to anaerobic states (hypoxia);[107] detect sweat glucose level for tracking blood glucose levels (diabetes);[108] analysis of sweat chloride, pH, and average sweat rate for obtaining insight into electrolyte balance, hydration status, and overall health conditions.[109–116] While long-term continuous monitoring of sweat is challenged by difficulties such as sensor signal drift and variations in interpretation of the concentrations, its advantages over other biofluids have rapidly promoted it to the forefront of skin-mountable health monitoring devices.[117–120] Traditional clinical methods involve collecting sweat by attaching either a disposable filter paper or a gauze pad to the skin, followed by benchtop determination and analysis of the concentration of sodium chloride (NaCl) through sophisticated laboratory instruments such as liquid chromatography, chloridometry, and mass spectroscopy. These methods have provided valuable practical means in many clinical contexts, but the accuracy of analysis remains limited by the loss, contamination and degradation of sweat samples during the required multiple steps of collection, storage, transport, and evaluation.[18]

Figure 4a (left) shows the most promising concept in the domain of miniaturized, flexible, and stretchable electronics that can be directly mounted on the human skin where the embedded electrochemical potentiometric and amperometric sensors provide real-time analysis.[14] The device exploits thin, soft microfluidic channels embedded with arrays of small circular (3 mm in diameter) and ellipsoidal (major axis, 6 mm; minor axis, 4 mm) openings in the inlet ports. This configuration allows freshly excreted sweat to be delivered into the compartmentalized microchambers where colorimetric sensors are deployed to detect chloride, pH, sweat rate, and total sweat loss. More specifically, the colorimetric chloride sensing occurs by using the mixture of silver chloranilate and poly (hydroxy ethyl methacrylate) solution that can generate a purple color-displaying chemical when complexed with chloride ion. The colorimetric pH sensing occurs by using a pH dye (Thermo Fisher Scientific, NH, USA) immobilized in the filter papers by dip-coating with the mixture of polyvinylchloride, o-nitrophenyl octyl ether, and Aliquat 336 in tetrahydrofuran. The colorimetric sweat rate/loss sensing occurs by which the incoming sweat dissolves a water-soluble dye, yielding a colored fluid.[121]

Electrochemical sensing simultaneously occurs to detect glucose and lactate in a mode where target analytes produce electrical signals proportional to their concentration. These features lead to eliminate the need of using bulky potentiostat, resulting in further miniaturization of the embedded computing components. The multimodal sensing capability is critical for comprehensive understanding and tracking of health status.

The device platform consists of two key components: i) a disposable soft, microfluidic network and ii) a reusable, thin near-field communication (NFC) electronic module (**Figure 5**a, middle). The hybrid assembly of the thin, soft microfluidics with the miniaturized rigid NFC modules provides advantages of comfort contact to the skin along with the entire range of sensing and wireless transmission of data to any NFC-enabled consumer handheld devices such as smart phone, smart tablet, and smart watch. The device incorporates a battery-free design by using a detachable, bilayer flexible circuit board (diameter: 18 mm, thickness: 0.5 mm) with a minimal component count for real-time data acquisition from the embedded lactate and glucose sensors located in the microfluidic structure (diameter: 32 mm, thickness: 1 mm). A commercial biocompatible adhesive (PC2723U, Scapa Healthcare) enables robust attachment of the device to the skin.

The corresponding field testing occurs on healthy, non-diabetic, and consenting human volunteers by attaching the device on the upper wrist, while the data were recorded in real time during physical exercises on a stationary bike. The results show that the device offers significant spatial latitude to the wearer for long-term data collection of sweat glucose and lactate levels over multiple days. The data provide good correlation with separate control analyses on blood lactate and glucose levels obtained by commercial instruments (Lactate Plus; Nova Biomedical, MA and Accu-Chek Nano Blood Glucose Meter; Roche Diabetes Care Inc.) (Figure 4a, right). Future directions for the practical implications would require further optimization of the device performance and systematic validation of its effectiveness in large clinical trials. Another great interest may exist in the use of the established materials and design layouts for extending the applications in tracking various diseases (diabetes, kidney diseases, and cystic fibrosis), pharmacokinetics, and the effect on pressure ischemia and stress markers.[122–124]

3.1.2. Sleep Monitoring

Monitoring of the skin temperature and pressure during sleep from specific areas of the body can facilitate the determination of human health status and also provide predictive information to prevent several diseases including sleep disorders.[125,126] For example, any variations of the skin temperature during sleep can be used to gauge the circadian phase, with important clinical implications for the characterization and treatment of common sleep disorders associated with delayed sleep-awake phase, advanced sleep-awake phase, and jet leg.[127] In addition, the measurement of the skin pressure while lying on a bed can provide critical information as an alert for the need of preventive action to avoid skin sores, irritation, and decubitus ulcers, which are often caused by sustained pressures on the skin for prolonged durations in a given posture.[128–130] Conventional
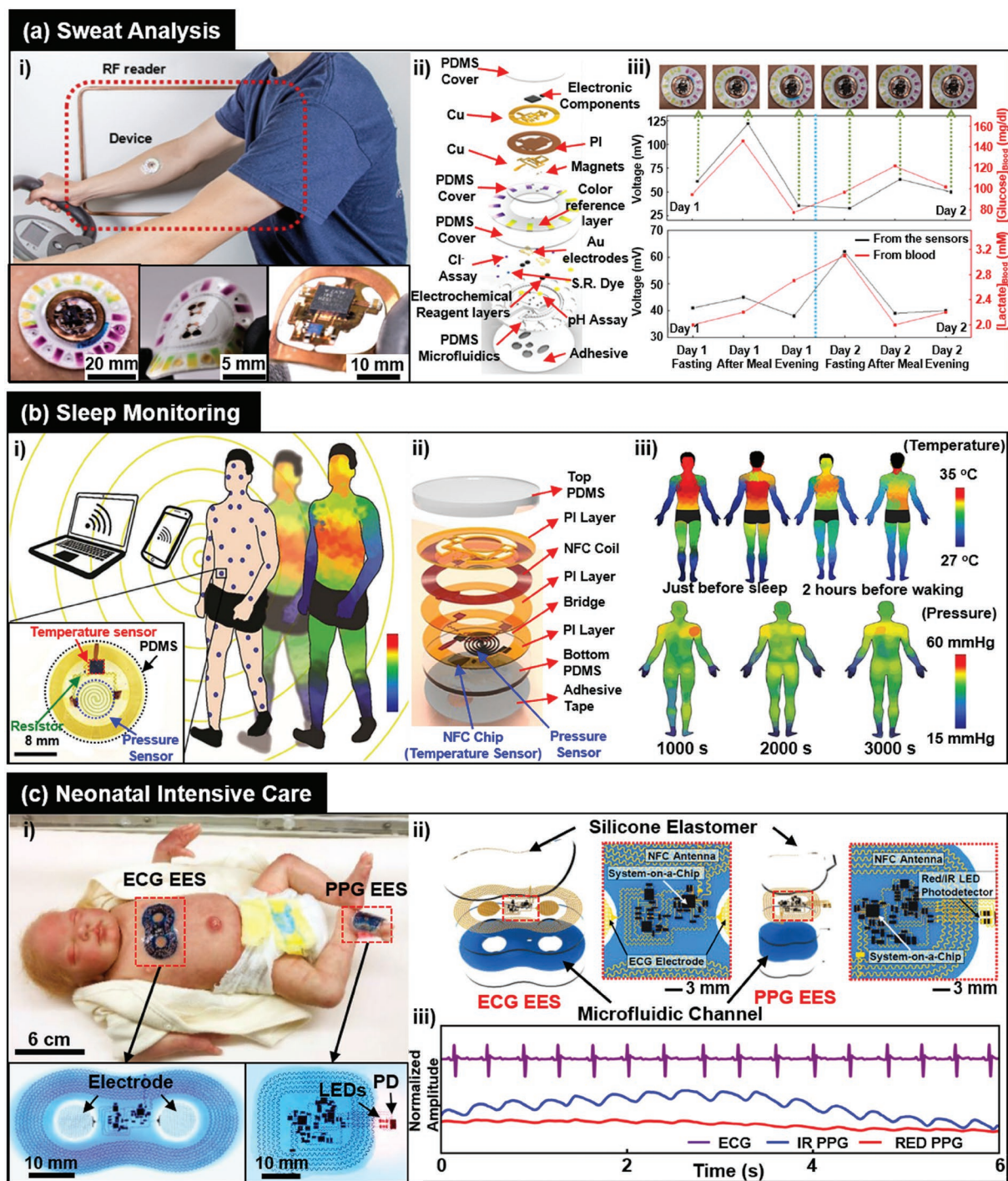
Figure 4. Skin-mountable health monitoring systems. a) Sweat analysis. i) A photo (top) of the miniaturized, flexible, wireless, and battery-free sweat sensor with close-up images (bottom). ii) The exploded view of the device configuration. iii) Correlation of glucose and lactate levels obtained from sweat against those collected from blood. a) Reproduced with permission.[14] Copyright 2019, The Authors, published by American Association for the Advancement of Science. Reprinted/adapted from *Science Advances* **2019**, *5*, eaav3294 © 2019, The Authors, some rights reserved; exclusive licensee American Association for the Advancement of Science. Distributed under a Creative Commons Attribution NonCommercial License 4.0 (CC BY-NC) http://creativecommons.org/licenses/by-nc/4.0/. b) Sleep monitoring. i) Illustration of the spatiotemporal mapping of the skin temperature and pressure across the body with top-view photo of the sensor. ii) The exploded view of the device configuration. iii) Experimental results of the temperature and pressure distributions across the body in a clinical sleep laboratory. b) Reproduced with permission.[15] Copyright 2018, American Association for the Advancement of Science. c) Neonatal intensive care. i) NICU setting with a life-sized neonate doll wearing two devices on the chest and foot for wireless monitoring of ECG and PPG, respectively. ii) The exploded view of the device configuration. iii) The recorded ECG and PPG data by the devices from a healthy term neonate. c) Reproduced under the terms of the CC-BY Creative Commons Attribution 4.0 International license (http://creativecommons.org/licenses/by/4.0/).[17] Copyright 2019, American Association for the Advancement of Science.

clinical methods on the sleep monitoring typically occur in a research laboratory that primarily relies on expensive, bulky sensing systems such as rectal probes, infrared (IR) camera, and pressure sensor-embedded mat.[131,132] These monitoring schemes, however, provide limited spatial resolutions of the measurements, and particularly, the IR monitoring can only examine the bare skin, impeding its practical use. In addition, these monitoring protocols require patients to make multiple visits to a clinical sleep laboratory for treatments, which would be difficult for many patients especially for those with mobility limitations or living in rural areas. Therefore, the need for accurate and inexpensive monitoring system for remote monitoring of the skin temperature and pressure across the body at high spatial resolution is high.

Figure 4b (left) shows the most promising concept in this regard in which multiple skin-mountable miniaturized wireless sensors are mounted across the human body over large-area in a spatially distributed manner, allowing for real-time spatiotemporal mapping of both the skin temperature and pressure.[15] The use of multiple separate devices across different locations of the body can expand the capability that enables simultaneous full-body monitoring of position-dependent body processes, disease states, and external stimuli. Figure 4b (middle) shows an exploded view of the device, of which the constituent components include: i) a resistance-based thermometer connected to a NFC chip for the detection of skin temperature, ii) a loop antenna for wireless power delivery and data communication to a central microcontroller unit, iii) a doped monocrystalline silicon membrane for the detection of skin pressure by exploiting its intrinsic piezoresistive property where the resistance changes upon applied strain, iv) a thin polyimide layer for electrical insulation, v) a silicone elastomer overcoat such as PDMS for encapsulation, and vi) a commercial biocompatible skin adhesive (thickness: ≈50 µm, mechanical modulus: ≈17 kPa, Scapa). Notably, the mechanically fragile Si membrane is configured into a spiral shape and overcoated with additional thin poly(ethylene terephthalate) (PET) to enhance the mechanical longevity as well as the uniformity in pressure-induced distribution of strain.

The corresponding field testing in the full-body thermography during sleep occurs in a clinical sleep laboratory by attaching total 65 devices across the body of a human subject, followed by continuous mapping of the full-body temperature at 20 times per min during the entire course of 9 h sleep. The results show that the core region of the body exhibits the skin temperature of 2–3 °C higher than the periphery, as expected by considering the distance from the heart (Figure 4b, right). The lowest body temperature occurs 2–3 h before waking, which is coincided with the fact that the body temperature begins to decrease at the onset of sleep (≈60 min) and then reaches the minimum value 2–3 h before waking. In parallel, the full-body mapping of the skin pressure takes place on 29 different locations across the dorsum of the subject lying on an adjustable hospital bed. The results also indicate that the average pressure exerted on the shoulder, buttock, and dorsum is increased as the supine angle of the bed is increased from 0° to 60°. These monitoring schemes in the full-body thermography and pressure measurements have a great potential in noninvasive, convenient, safe, and comfort diagnosis of sleep disorders and/or

prevention of skin sores and decubitus ulcers. Future directions for the practical clinical implications would require further optimization of wireless techniques and antenna design not only to increase the operating range (30–40 cm) but also decrease the required power (several watts). Extensive human trials beyond the product developments would be also necessary for validation in clinical settings.

### 3.1.3. Neonatal Intensive Care

Approximately 300 000 neonates each year in U.S. only are admitted to neonatal intensive care units (NICUs) due to prematurity and low birth weight below 1500 g.[133] The NICUs require comprehensive monitoring for collecting data of various vital signs such as heart rate, respiratory rate, temperature, blood oxygenation, and peripheral capillary oxygen saturation (SpO$_2$).[134,135] However, currently used monitoring devices provide rigid or semiflexible form factors, yielding large mechanical mismatch with the soft, curvilinear surface of the neonatal skin. In addition, these devices are connected with multiple wires for powering and data acquisitions, and thereby often require strong adhesion of the devices onto the exceptionally fragile neonatal skin.[136–140] This inevitably yields unfavorable environments for neonatal care because: i) turning a neonate from prone to supine is difficult, ii) the skin-mounted devices interfere with emergency clinical interventions and radiological examinations, iii) therapeutic skin-to-skin contact between parents and their infant (i.e., kangaroo care) is impeded, and iv) strong adhesion between the device and the fragile neonate skin causes iatrogenic injuries and subsequent scarring. A potential risk also exists in inadvertent separation of rigid sensors from the neonatal skin particularly by natural motions of the neonate, which may result in inaccurate data collection or false alarm. Moreover, these devices remain consistently expensive, impeding their wide use, and adoption in low-income settings. These circumstances greatly motivate the development of a noninvasive, nonintrusive, accurate, and inexpensive monitoring system for efficient neonatal intensive care.

Figure 4c (left) describes recent development of a wireless, battery-free and skin-mountable monitoring device that incorporates a bimodal pair of ultrathin, low-modulus measurement modules, providing the ability to softly and noninvasively interface with the neonatal skin.[17] The monitoring system includes two different types of skin-mountable sensors that contain a collection of thin, narrow serpentine metal traces for the interconnection of multiple, chip-scale circuit components (Figure 4c, right top).[141] One device is to be mounted on the chest to record electrocardiograms (ECGs) through the skin-interfaced electrodes consisting of filamentary metal mesh structures in fractal geometries.[106,142] The other is to be mounted on the base of the foot to record photoplethysmograms (PPGs) by reflection-mode measurements with aid of a photodiode and a pair of LEDs, which emit red (640 nm) and infrared (940 nm) lights.[143] The measurement of PPGs involves the determination of volumetric changes in blood vessels or organs by illuminating the lights onto the skin and detecting the reflected amount to a photodiode, providing

ADVANCED
SCIENCE NEWS
www.advancedsciencenews.com
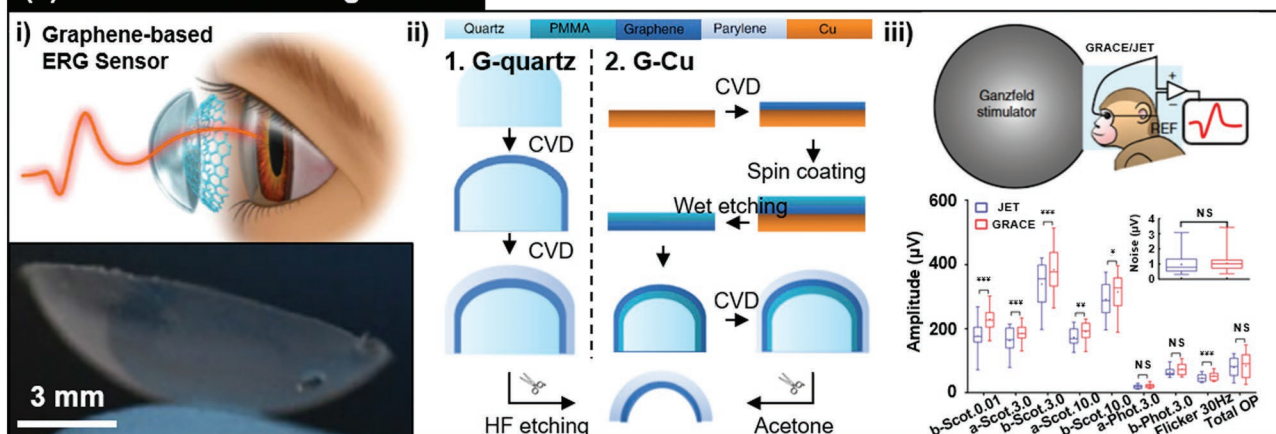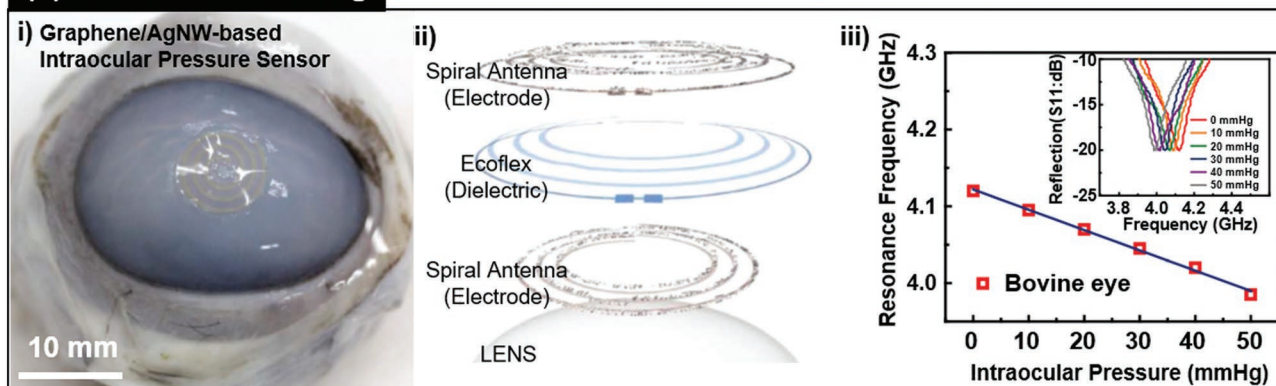
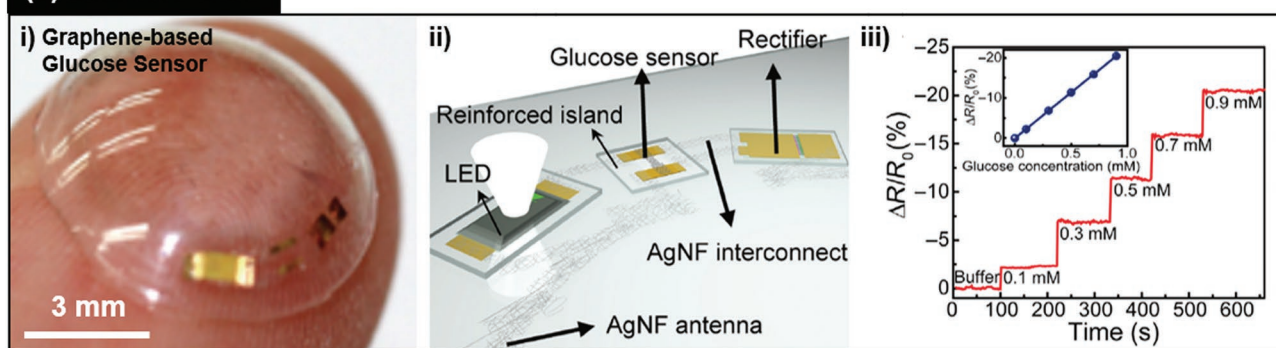ADVANCED
MATERIALS
www.advmat.de

Figure 5. Eye-mountable health monitoring systems. a) Retinal disorder diagnostics. i) Schematic illustration of the recording of ERG signals with the graphene-based G-quartz device with a close-up photo of the device. ii) Schematic illustration of the fabrication procedures for the G-Cu and G-quartz devices. iii) Schematic illustration (top) of the recording of ERG signals with ganzfeld stimulation on a cynomolgus monkey, and experimental results (bottom) for the comparison of various ERG responses with the G-quartz device and conventional JET electrodes. a) Adapted under the terms of the CC-BY Creative Commons Attribution 4.0 International License (http://creativecommons.org/licenses/by/4.0/).[162] Copyright 2018, The Authors, published by Springer Nature. b) Glaucoma Monitoring. i) A photo of the graphene/AgNW-based contact lens device placed on a bovine eyeball. ii) The exploded view of the device configuration. iii) The recorded frequency response by exerted pressure obtained with the device placed on the bovine eye. b) Adapted under the terms of the CC-BY Creative Commons Attribution 4.0 International License (http://creativecommons.org/licenses/by/4.0/).[30] Copyright 2017, The Authors, published by Springer Nature. c) Diabetes care. i) A photo of the graphene-based contact lens device. ii) Schematic illustration of the device configuration. iii) Continuously measured glucose level depending on concentrations (inset: calibrated data). c) Adapted with permission.[31] Copyright 2018, The Authors, published by American Association for the Advancement of Science. Reprinted/adapted from *Science Advances* 2018, 4, eaap9841 © The Authors, some rights reserved; exclusive licensee American Association for the Advancement of Science. Distributed under a Creative Commons Attribution NonCommercial License 4.0 (CC BY-NC) http://creativecommons.org/licenses/by-nc/4.0/.

many clinically useful information including heart rate, heart rate variability, respiration rate, blood oxygenetaion, and pulse arrival time.[144] A key feature of the sensors involves the use of a nontoxic ionic liquid (1-ethyl-3-methylimidazolium ethyl sulfate) that is inserted between the electronics and the lower encapsulation layer, allowing the interconnected components to be mechanically isolated from the neonatal skin.[145] A thin layer of soft overcoat such as PDMS provides the compatibility with NICU incubators where the internal humidity is commonly above 80%.[146] The inherently thin, soft nature of the devices (effective moduli: 200–300 kPa) results in minimal normal and shear stresses at the interface with the neonatal skin even under natural motions of a neonate. In addition, the devices contain a magnetic loop antenna for wireless data transmission and power delivery through NFC protocols, enabling continuous real-time recording of ECG, PPG, and skin temperature from a distance.

The corresponding field preliminary testing of the ECG and PPG monitoring occurs on both healthy neonates and premature infants in two tertiary-level NICUs. The ECG sensors are mounted on the chest or on the back to facilitate chest-to-chest skin interaction between parent and neonate. The PPG sensors are mounted on the base of the foot or on the upper limb for optional placement. The results show that the continuously recorded and postprocessed data of heart rate, respiration rate, and SpO_2 are consistent with the control monitoring using gold-standard equipment (Intellivue MX800, Philips) operating concomitantly. Further validations on three neonates ranging in gestational age from 28 to 40 weeks admitted to the NICU show strong agreement in the heart rate, respiration rate, and SpO_2 with negligible mean difference. In addition, time-synchronized outputs from the ECG and PPG sensors allow for the determination of pulse arrival time and continuous differential skin temperature (Figure 4c, right bottom), which presents advanced physiological parameters and valuable clinical information which otherwise cannot be regularly collected in routine practices in NICUs.[147,148] The devices successfully reproduce comprehensive vital signs and exhibit high mechanical and noninvasive skin adhesive interface, water resistance, and the compatibility with essential medical imaging and inspection.

3.2. Eye-Mountable Monitoring Systems

Since the first conceptual invention by Leonardo da Vinci in the 16th century, there has existed great desires in the use of contact lenses for eye-mountable biomedical platforms owing to the simple and noninvasive accessibility to the body's internal chemistry (tear film) and the eye's outermost layer (cornea).[1,4,149–151] Nevertheless, current contact lenses serve only either to correct vision problems or to deliver ocular drugs in a passive manner.[152] Recent technological advances allow the advent of several proof-of-concept contact lens-based eye-mountable sensors for noninvasive and continuous monitoring of metabolites in tear film such as glucose and lactate.[30,31,153–158] The eye-mountable platform also possesses a great potential for continuous monitoring and early diagnosis of ocular diseases such as glaucoma, cataract, and retinal

diseases.[30,159–162] The following sections introduce several representative examples of the eye-mountable health monitoring devices by categorizing them into its clinical implementation in: i) retinal disorder diagnostics, ii) glaucoma monitoring, and iii) diabetes care (Figure 5).

3.2.1. Retinal Disorder Diagnostics

Among various electrophysiology that can help diagnose the status of eye(s), electrical recording of full-field electroretinogram (ERG) has been widely used to understand the electrical activity generated by photoreceptors in the retina in response to light stimuli.[163–166] A most common conventional clinical method involves placing a recording electrode shaped into either loops, hooks, or wires on the bulbar conjunctiva while stimulating the eye with a bright light source such as a flash produced by light-emitting diodes (LEDs) or a strobe lamp.[167,168] The monitoring of ERG signals from the bulbar conjunctiva naturally prevents the recording electrodes from direct physical contact with the exceptionally sensitive corneal surface, and thereby can reduce discomfort and promote eye movement during examination.[167,168] However, the amplitude of ERG signals is typically weak and its stability and reproducibility are compromised. Alternative methods involve the use of a contact lens featured with metal conductors on the peripheral area in which this configuration allows the light to be transmitted through the center area.[169,170] In the monitoring scheme, the recording electrode remains contacted with the corneal surface and provides relatively high amplitude of ERG signals, but it inevitably induces severe discomfort of the wearer caused by the large mechanical mismatch between the stiff, flat metal electrode and the soft, curvilinear corneal surface. This consequently leads to the use of auxiliary blepharostat for supporting the strict coral contacts. Therefore, the need for mechanically soft and optically transparent eye-mountable sensor for noninvasive, comfortable, and accurate recording of ERG signals is high.

Figure 5a (left) describes a recent development of a graphene-based contact lens device that provides broadband optical transparency (71.7% at 550 nm), low sheet resistance (≈1520 Ω sq^{-1}), and electrochemical impedance (4.85 ± 0.36 kΩ at 100 Hz).[162] This device consists of 5–25 µm thick Parylene-C to serve as the soft and transparent substrate configured into a contact lens shape, of which the concave side is laminated with graphene electrode grown by low-pressure chemical vapor deposition (LPCVD). The graphene can be grown on the substrate in two ways, either on the lens-shaped quartz glass directly (G-quartz) or on a flat copper foil and then transferred to a lens-shaped quartz mold (G-Cu) (Figure 5a, middle). The G-Cu exhibits better properties in term of the optical transparency of 83.8% at 550 nm, the sheet resistance of ≈850 Ω sq^{-1} and the electrochemical impedance of 3.39 ± 0.30 kΩ at 100 Hz, but folding or wrinkles of the graphene typically appear during the transfer printing process due to the mechanical mismatch between the flat G-Cu and the curvilinear surface of the contact lens.[171–173] On the other hand, the G-quartz provides improved uniformity in terms of the thickness across the entire electrode surface, but the optical transparency and electrical conductivity are

**ADVANCED
SCIENCE NEWS**
www.advancedsciencenews.com

**ADVANCED
MATERIALS**
www.advmat.de

limited. The recording of the ERG signals involves the use of the G-quartz electrode due to its ability to establish highly conformal interface with the curvilinear corneal surface and avoid the formation of air gaps or inhomogeneous tear film between the electrode and cornea. These aspects allow for the high-resolution and high-fidelity acquisition of ERG signals.

The corresponding field preliminary testing of the ERG monitoring occurs on a cynomolgus monkey. After anesthetizing, the eyes are dilated and worn with G-quartz devices, followed by recording with an illumination of short flashes and/or steady background light into the eye evenly by using a Ganzfeld stimulator (Figure 5a, right top).[174] The subcutaneous reference and ground electrodes are placed at a posterior region to the lateral canthus and at the tail, respectively. The results indicate that the amplitude of the ERG signals from the G-quartz-based device is higher than that from conventional ERG Jet electrode made of plastic lens-shaped speculum in spite of approximately seven times higher impedance of the G-quartz, mainly because the soft and lightweight G-quartz-based device yields a conformal contact to the corneal surface and forms a tight interface with thinner tear film than the Jet electrodes. The measured multifocal ERG (mfERG) responses provide statistically comparative results with those obtained from the control measurements (Figure 5a, right bottom). The results confirm that the waveform of the mfERG responses resembles typical waveform of photopic flash ERG with an initial negative deflection followed by a positive peak, wherein the highest signal amplitude occurs in the central regions of the cornea due to the highest density of retinal cone. This study successfully demonstrates a unique eye-mountable platform that can provide mechanical softness, optical transparency, and capability for monitoring various ERG signals, suggesting its future directions for research on ocular electrophysiology and practical clinical uses.

3.2.2. Glaucoma Monitoring

Abnormal increase of intraocular pressure can damage the optic nerve and can result in glaucoma.[175] Approximately 79.6 million people worldwide are reported to experience glaucoma, and more than 11 million of them become consequently bilaterally blind.[176] According to the National Eye Institute (NEI), early detection, diagnosis, and monitoring of glaucoma can often prevent from serious vision loss. Elevated intraocular pressure (IOP) is the largest risk factor for glaucoma and, without proper treatment, can lead to progression of the disease in ≈70% of all glaucoma cases.[161,175,177] Although the intraocular pressure peak occurs at night rather than daytime, it is frequently measured when patients visit a hospital during daytime due to the time and place limitations.[161] Therefore, continuous recording of IOP during day and night by using an eye-mountable monitoring system is highly attractive, as also evidenced by recently increased number of reports related to the eye-mountable IOP sensors.[178,179]

Figure 5b (left) describes a notable recent example of the contact lens-based IOP sensor that employs a stretchable and transparent capacitive sensing element.[30] The device exploits a capacitive sensing mode that is suitable for measuring small forces, which becomes more favorable for the IOP sensing than strain sensing.[161] The sensing components act as resistance, inductance, and capacitance circuit operating at the radio frequency of 3.95–4.15 GHz, which enable the wireless, real-time acquisition of data without additional power source and associated circuitry. The IOP sensing occurs wirelessly by using an external reader coil aligned along the same axis with the device. Specifically, the distance between the reader coil and the device is ≈1 cm in which their inductive coupling allows for the analysis of how the reflection condition depends on the capacitance and inductance change of the sensor.

The device consists of silicone elastomer (Ecoflex) as a dielectric layer sandwiched between two inductive spiral graphene–silver nanowires (AgNWs)-based hybrid electrodes (Figure 5b, middle). The elevation of intraocular pressure leads to a substantial increase of corneal radius of curvature, thereby resulting in the increase of capacitance and inductance by thinning the dielectric layer and expansion of spiral coils, respectively. The graphene–AgNW hybrid electrodes provide sufficient optical transparency (>80% in visible range) and mechanical stretchability at the applied tensile strain of ≈25%, allowing the device not only to be transferred onto the curved surface of a contact lens without suffering any defects or damages, but also to provide comfort and unobstructed vision for the wearer.

Preliminary ex vivo evaluation occurs on an extracted bovine eyeball which size and structure are similar to those of human eyeballs (21–27 mm in diameter). The results indicate that the resonance frequency of the capacitor is down-shifted at higher IOP that leads to increase of the corneal radius of the curvature, thereby increasing both the capacitance by thinning the dielectric and the inductance by biaxial lateral expansion of the spiral coils (Figure 5b, right). The frequency responses are nearly linear at the IOP below 50 mmHg with negligible hysteresis. Comprehensive in vivo clinical studies are required to confirm the correlation between the measured pressure and the IOP while further improvement of the wireless operational distance (≈1 cm) would be also necessary for the clinical trials.

3.2.3. Diabetes Care

Diabetes, causing uncontrollable blood glucose levels, is one of the most prevalent chronic diseases for more than 382 million people worldwide, which is continuously on the rise.[180] A common traditional clinical method involves the use of a sharp needle that can prick the fingertip or other parts of the body to gain a blood drop for subsequent benchtop analysis of blood glucose levels.[181] Even though patients with diabetes are generally advised to check their blood glucose level daily, this method yields pain during the needle pricking and accompanying intense stress of repetitive blood collection. Therefore, a minimally invasive approach for painless and stress-less glucose monitoring is highly desired, justifying the current numerous research efforts on the continuous point-of-care monitoring of glucose levels over time for efficient management of diabetes.

Recent technological developments have enabled the advent of proof-of-concept instrumented contact lenses (e.g., the Google's smart contact lens) that are tailored for continuous monitoring of glucose level in the wearer's tear film.[152,182] This

**ADVANCED
SCIENCE NEWS**
www.advancedsciencenews.com

**ADVANCED
MATERIALS**
www.advmat.de

eye-wearable monitoring scheme is attractive because the collection of tear films occurs in a natural way through normal secretion and eye blinking. These developments provide the rationales to fuel the relevant research field, but key challenges still remain in the fact that the instrumented contact lenses are fabricated on a custom-made contact lens that is made of materials that can tolerate the fabrication conditions for sensors and electronics, typically by using transparent plastics or a few kinds of polymers such as PETs and parylene-C.[156,162,183] Consequently, the resulting devices offer limited oxygen and water permeability (short-term wearability), wettability (dryness), and softness and ergonomic design (discomfort), thereby impeding their practical uses. In addition, the challenges related to the signal drift in long-term monitoring as well as the variations in interpretation of the biomarker concentrations remain to be overcome for its clinical practices.

Figure 5c (left) describes an example of the current state-of-the-art contact lens-based device for continuous monitoring of glucose level from tear films,[31] providing several advanced features: i) The device platform consists of a soft contact lens with highly transparent and stress-tunable hybrid structures for ensuring the device reliability and wearer's view, ii) The overall device layout incorporates "device island/serpentine interconnector" configurations that can control strains under stretching for which the "islands" that include sophisticated electronic components can withstand negligibly small strains while mechanically robust, stretchable "interconnectors" can accommodate most of the strains,[184–186] iii) The device incorporates a LED pixel for remote display of sensing information in real time and iv) The wireless operation occurs without noticeable heat generation, allowing the corneal surface to remain stable. Specifically, glucose oxidase (GOD) and catalase immobilized on a graphene transistor channel are used as an active sensing element for the selective and sensitive detection of glucose by which the oxidation of glucose by GOD yields H_2O_2, and further oxidation of the H_2O_2 via electrochemical reaction releases electrons, resulting in the increase of the drain current of the graphene transistor.[187] The use of catalase is to improve the sensitivity of the sensor (the measurable glucose level up to 0.9×10^{-3} M) by increasing the enzymatic activity of GOD.[188] The LED pixel is to indicate when the glucose concentration is detected above the typical glucose concentration (0.9×10^{-3} M) in the tear films of patients with diabetes.[189] The integrated Ag nanofiber antenna and rectifier are to provide wireless power transmission from an external power source to the device and convert the received AC signal into DC for driving the LED. A schematic illustration of the key electronic components for this device appears in Figure 5c (middle).

To validate the effectiveness, in vivo evaluation occurs on a rabbit model by gently placing the contact lens device on the eye and powering through an external inductive coil from the distance of ≈5 mm. The LED is turned off when the glucose concentration is increased above 0.9×10^{-3} M. Throughout the examination, the temperature of the contact lens is maintained at ≈37 °C without any significant heat generation while the rabbit shows no signs of abnormal behaviors when the LED is turned on and off. A set of data obtained from these preliminary tests provides substantial promise of future improvements

and implementation of the devices in clinical trials. A key challenge, however, remains to be overcome in the fact that the electrochemical reaction produces by-products including H_2O_2 that are harmful to eye. Follow-up investigations would be also necessary to reveal the accurate correlation of the glucose levels between tear films and bloods.
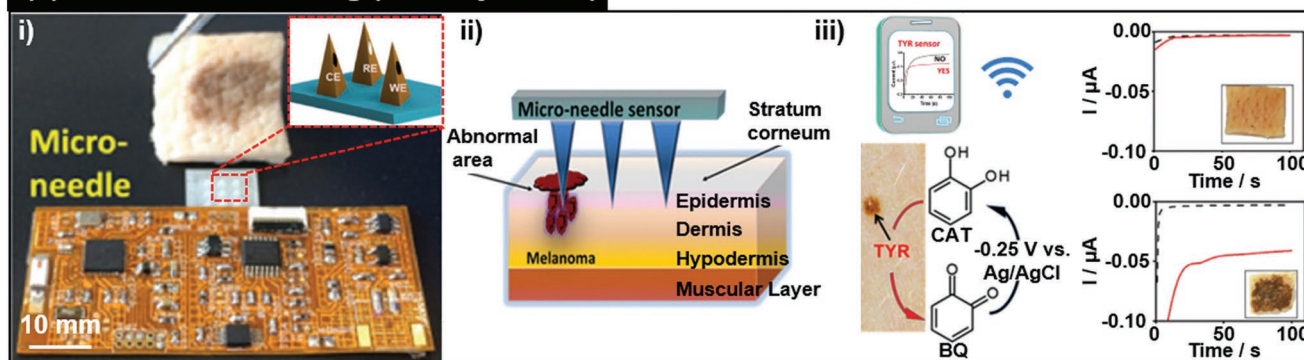
3.3. Skin- or Eye-Injectable Monitoring Systems

Tissue-injectable sensors that can penetrate the skin or eye by means of needles provide the ability to access and analyze the internal body electrophysiological activities and chemistries, which otherwise cannot be achieved by using the surface-interfaced sensors. These injectable monitoring can capture the electrophysiological signals from organs and neurons as well as the concentration of electrolytes, salts, glucose, and lactate from interstitial fluids and bloods, providing many advantages over the other indirect measurements in terms of accuracy and capability of the real-time monitoring without significant time lag.[190–194] These injectable sensors have emerged to serve as alternatives to implantable devices for less invasive and unobtrusive monitoring, and thereby eliminating the need of any surgical procedures. Various forms of injectable devices including transdermal microneedle sensors[190,191,195,196] and syringe-injected ultraflexible mesh sensors[197–202] have been demonstrated by exclusively using biocompatible materials that can minimize the local inflammation and scar tissue. The following sections introduce several representative examples of the skin- or eye-injectable biomedical devices by categorizing them into its clinical implementation in: i) melanoma screening and ii) neurological disorder monitoring (**Figure 6**).

3.3.1. Melanoma Screening

The incidence of melanoma skin cancer, the most fatal form of skin cancer, is increasing faster than any other potential preventable cancer, which becomes the 5th most commonly diagnosed cancer in men and 7th in women in the U.S.[203] Melanoma is an aggressive skin cancer, and thereby the early detection and recognition is critical for reducing the mortality. The most common traditional screening method for melanoma includes both self-examinations and professional skin exams of asymptomatic individuals to identify suspicious lesions that require further evaluation. Self-examination is typically recommended at least once a month in front of the mirror prior to professional skin exam to identify any lesions that might be cancerous or precancerous. The subsequent professional skin exam involves the use of sophisticated monitoring such as immunohistochemical staining to detect melanocytic lineage markers, but includes time-consuming and complex procedures.[203–206] A clinical biomarker in melanoma, tyrosinase (TYR), is a polyphenol oxidase, which participates in synthesis of melanin, and its accumulation above the average is known to induce melanoma.[207,208] The detection of TYR provides a great clinical role for the screening of primary melanoma with its sensitivity of nearly 100%, but the efficacy becomes reduced when the disease progresses.[209] The cancerous tumor begins
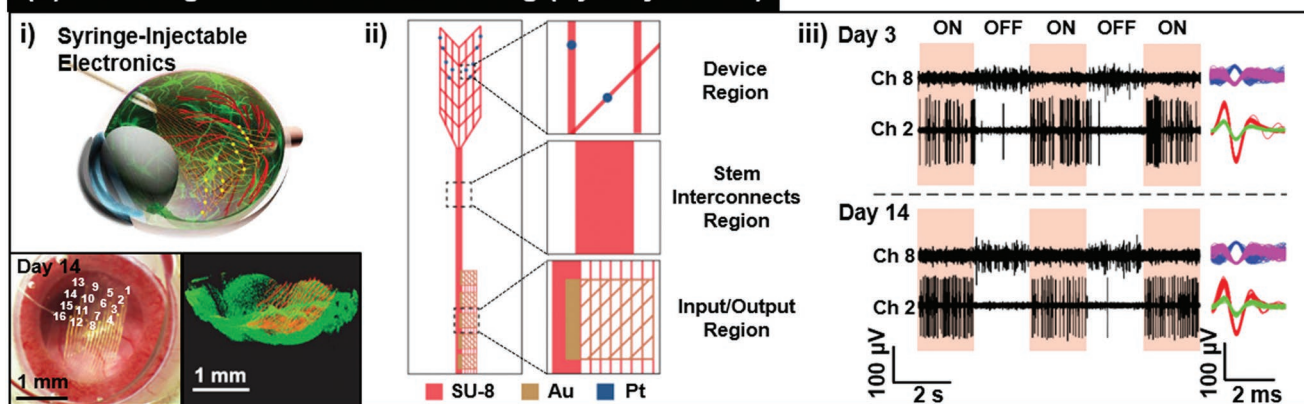
Figure 6. Skin- or eye-injectable health monitoring systems. a) Melanoma screening (skin-injectable). i) A photo of the microneedle-based sensor integrated with a wireless unit. (inset: The schematic of the pyramidal microneedles for the working, counter, and reference electrodes). ii) Schematic illustration of the transdermal detection of TYR biomarker by using the microneedle sensor. iii) TYR sensing mechanism and amperometric response of the microneedle-based sensor before (dotted black) and after (red) interaction with untreated (top) and 2.5 mg mL^{-1} TYR-treated (bottom) pork samples. a) Adapted with permission.[210] Copyright 2018, Wiley-VCH. b) Neurological disorder monitoring (eye-injectable). i) Schematic illustration (top) for the noncoaxial intravitreal injection of the ultraflexible mesh device onto the epiretinal region, with the in vivo through-lens image (bottom left) of the mouse eye fundus on day 14 after the injection and the ex vivo image (bottom right) of the injected device (red) and the RGCs (green). ii) Schematic illustration of the device configuration. iii) Recorded light responses from the two representative channels on day 3 and 14 after the injection. Images in (b-i,iii): Adapted with permission.[202] Copyright 2018, American Association for the Advancement of Science. Images in (b-ii): Adapted with permission.[219] Copyright 2018, The Authors, published by MyJove Corp.

to form just above the dermis ($\approx$250 µm from the top surface of epidermis) where melanocyte cells are located and produce the skin's pigment. These circumstances make the transdermal injection of a sensor to the dermis attractive for accurate screening of melanoma.

Figure 6a (left) describes a skin-injectable sensor that incorporates an array of microneedles embedded with electrochemical sensing elements for the detection of TYR.[210] Specifically, a 3 × 3 array of 800 µm long polymeric hollow microneedles are injected through the skin moles until the needle tips reach the infected melanoma tissues where TYR presents (Figure 6a, middle). The microneedles are filled with carbon paste made of graphite powder and mineral oil where the surfaces are coated with catechol/agarose solution. This configuration allows the microneedles to overcome the stratum corneum barrier and then detect TYR in the transdermal tissues of the skin moles while simultaneously ensuring minimal pain and distress. The sensing mechanism is relied on electrochemical and amperometric detection in which it can distinguish the

reduction of electrical currents against the Ag/AgCl reference electrode while the catechol is oxidized into benzoquinone (BQ) in presence of TYR. Wireless streaming of the data to an external mobile device such as a smartphone is available by using additional electronic unit (50.8 × 24.1 mm) made of a polyimide-based flexible printed circuit board (PCB) that contains miniaturized potentiostatic circuits and Bluetooth modules.

For ex vivo evaluations, the microneedles are injected into the porcine skin that provides structural similarity to the human epidermis in terms of thickness, dermal-epidermal thickness ratio and TYR content. Prior to the injection, a portion (1 × 1 cm^2) of the porcine skin is dosed with different concentrations of TYR where the skin color is changed from pink (untreated) to dark brown (2.5 mg mL^{-1}). The results clearly show the distinguishable reduction of the currents occurred when injected into the porcine skin with different dosages of TYR, whereas no responses appear when injected into the untreated control porcine skin (Figure 6a, right). The

**ADVANCED
SCIENCE NEWS**
www.advancedsciencenews.com

**ADVANCED
MATERIALS**
www.advmat.de

microneedle sensor can also discriminate different levels of TYR in the skin tissues, all in a wirelessly controlled fashion. This study successfully demonstrates the initial skin-injectable sensor platform that can offer an attractive analytical performance for early screening of melanoma through the skin moles. Several challenges still remain in the lack of fully miniaturized and flexible form factor for the powering and antenna units, suggesting the directions for future research.

3.3.2. Neurological Disorder Monitoring

Tissue-injectable sensing electrodes offer important opportunities for recording electrical impulses of brain activity, revealing the encoded information inside the brain for management of chronic neurological diseases such as Parkinson's diseases.[211] In particular, single neuron electrophysiology is clinically important for applications ranging from improved decoding algorithm performance for brain–machine interfaces to understanding and potentially predicting epileptic seizures.[201,212–215] Conventional approaches by exploiting injectable forms of neural sensing probes, due to their significantly high bending stiffness (>100 000 times of brain tissue), large size (>4 times of a single neuron cell body), and topological mismatch, are challenged in their capability to cover large spatiotemporal range (i.e., from the spatial scale of individual synapses/neurons with millisecond time resolution to that of neural networks comprising different brain regions evolving over months to years) and secure long-term stability related with chronic gliosis and mechanical mismatch with soft tissues.[216–221] For an instance, analysis of retinal ganglion cells (RGCs) that are responsible for receiving the neuronal signals from photoreceptors and then sending the information to visual areas of the brain remains limited by lack of effective method. Conventional approaches are mostly relied on ex vivo electrophysiological recording and calcium imaging, yielding difficulty in correlating retinal activity with organismic responses or behaviors with short recording time due to the lifetime of rod function in explants.[222–226]

To overcome these challenges, a paradigm-shifting approach has been recently demonstrated by delivering syringe-injectable ultraflexible mesh electronics into awake mice for chronical monitoring of neurological disorders at single-RGC resolution (Figure 6b, left).[202] The device is configured into ≈90% of macroporous structure in a 2D layout in order to accommodate the interpenetration of neurons and molecular diffusion with tissue-like mechanical properties, thereby minimizing physical damages and immune responses postinjection. The unique structural and mechanical properties of the device provide the ability to seamlessly interface with the retinal tissues, allowing for 3D interpenetration through the intact central nervous networks. The device consists of total 16 recording electrodes, polymer-encapsulated metal interconnect lines, and input/output connecting pads from/to an external data acquisition system, all of which is fabricated by standard photolithography and transfer printing method (Figure 6b, middle). Highly porous mesh structures with the characteristic width of <10 µm are designed to be injected and penetrated into an eyeball with minimal interference with the retina.

For in vivo validation, the device is injected into the epiretinal region of awake mice via noncoaxial and minimally invasive intravitreal injection through the lateral canthus with a glass capillary needle (outer diameter: ≈330 µm). For electrical recording, intracortical grounding and reference electrodes are used by which the input/output pads expelled out of the mice are connected to a 16-channel flexible flat cable (FFC) bonded with a carbon nanotube ink. The entire FFC with mesh electronics is then cemented to the mice skull for stable measurement. Recording is performed by restraining the mice with the head-plate in order to reduce mechanical noise during recording and fix the visual field of the recorded eye during light stimulations. The high-quality recording of RGC activity is obtained from all of the 16 channels, providing the signal-to-noise (SNR) ratio of >7. Importantly, no significant variation in the SNR occurs throughout the measurements for the two specific channels on days 3 and 14, suggesting the chronic recording stability (Figure 6b, right). In addition, the measurement on 32 RGCs (15 of nondirection-selective, 14 of direction-selective, and 3 of orientation-selective ganglion cells) in response to moving grating light stimulations and the investigation on circadian modulation of 28 RGCs indicate that various types of RGCs can be tracked for >2 weeks, revealing circadian rhythms in RGC responses over multiple day/night cycles with high fidelity. Consequently, the syringe-injectable ultraflexible sensors can serve as a potential alternative to the conventional injectable techniques, offering novel insights into dynamic information processing between retina and other parts of the central nervous system (CNS). Further optimization is possible by increasing the number of electrode channels and modifying the electrode design for full coverage of the retinal cup, and thereby can yield larger scale mapping of the retina neural circuitry.

4. Concluding Remarks

This report captures the wide-ranging and rapid developments of advanced flexible materials and hybrid printing techniques for their use in the human skin and eye-interfaced health monitoring systems that can leverage the benefit of demanding connected healthcare systems. The hybrid use of the printing materials and techniques discussed herein can circumvent the incompatibility between conventional microfabrication processes and flexible and biocompatible substrates, thereby significantly broadening the classes of printed electronics. **Table 3** summarizes the printing materials and techniques utilized for the construction of the exemplary devices discussed in this article.

The thin, flexible, and stretchable nature of the printed electronics allows for noninvasive wearable or minimally invasive injectable access to the skin, cornea, retina, and internal bodyfluids such as sweat and tears. The in-sensor data processing and wireless data and power transmission can be effective through the hybrid assembly of the flexible electronics with miniaturized rigid silicon-based microchips. The collective set of biosignals obtained wirelessly from a remote distance also provides potential benefits to home-based telehealthcare services and thereby alleviate the burden of frequent visits to hospitals and clinics, which can better help patients, doctors, and caregivers manage their therapies and treatments.

Table 3. Summary of the employed printing materials and techniques for the construction of the exemplary devices in Section 3.

Printing methods	Clinical applications	Printing materials and techniques	Refs.
Sacrificial layer etching-based transfer printing	Sleep monitoring device (Figure 4b)	Transfer of the p-doped monocrystalline silicon membrane (pressure sensing elements) through the chemical etching of the buried oxide (SiO_2) layer from a commercial silicon-on-insulator (SOI) wafer	[15]
	Retinal disorder diagnostic device (Figure 5a)	Transfer of the PMMA/graphene through the chemical etching of the bottom Cu foil	[162]
	Glaucoma monitoring device (Figure 5b)	Transfer of the intraocular pressure sensor (parylene/AgNW spiral coil/ecoflex/AgNW spiral coil/parylene structure) through the chemical etching of the bottom Cu foil	[30]
	Diabetes care device (Figure 5c)	Transfer of the wireless display-integrated hybrid substrates (SPC-414/elastofilcon A and SU-8/elastofilcon A) through the chemical etching of the bottom 800 nm thick Cu layer on a silicon substrate	[31]
	Neurological disorder monitoring device (Figure 6b)	Transfer of the mesh electronics (SU-8/Cr/Au/Pt/SU-8 structure) through the chemical etching of the bottom 100 nm thick Ni layer on a silicon substrate	[202]
Interfacial layer delamination-based transfer printing	Sweat analysis device (Figure 4a)	Delamination of the 200 μm thick PDMS slab (the microfluidic platform) from the bottom PMMA/silicon substrate.	[14]
	Sleep monitoring device (Figure 4b)	Delamination of wireless NFC sensors (PI/Cu/PI structure) from the PDMS/glass substrate using a water-soluble tape (Aquasol Corporation, ASWT-2)	[15]
	Neonatal intensive care device (Figure 4c)	Delamination of the 50 μm thick PDMS slab (the microfluidic platform) from the bottom fluorinated polymer (antiadhesive)-coated SU-8 mold	[17]
3D Printing	Melanoma screening device (Figure 6a)	3D printing of the 3×3 pyramid-structured microneedles with a photocurable acrylate-polymer material (Eshell 200 Envision, TEC GmbH)	[210]

A most attractive advantages of these printed electronics involves their cost effectiveness as the overall cost of printing process and infrastructure is low comparing to conventional fabrication methods for microelectronics and sensors. It is also desired to integrate the printing process with an existing roll-to-roll (R2R) manufacturing platform,[24] thereby allowing for the continuous, high throughput production of printed electronics on large rolls rather than batch processing wafers. This could potentially offer disposable health monitoring systems that can be widely adopted for many peoples in need including those in low-income communities. Several shortcomings of the printed electronics arises from the fact that the thin, flexible substrates are overly frangible and fragile while the additional coating of protective encapsulation layers increases the cost and thickness of the overall structure. The most formidable challenge also remains in the potential for unpredictable catastrophic failures of such flexible printed electronics by inadvertent overstretching or overbending beyond the fracture limits.[227]

These advances have enabled a broad range of novel biomedical applications for management of several diseases and disorders encompassing a group of conditions that require continuous monitoring of personal health data and biomarkers. Several of these devices have nearly reached at consumer level in which measurement accuracy, response time, selectivity, variability, reliability, chronic stability, and their clinical correlation are proven through extensive tests on human subjects. For future improvements, the remote data acquisition systems discussed in this article would require improved graphical user interface (UI) designs, which better help patients and clinicians to interpret the measured data and obtain clinically useful feedbacks. Many other future opportunities exist for improving both clinical decision support and caregiver support with aid of algorithms, apps, artificial intelligence (AI), and machine learning, along with software-defined and cloud-based digital infrastructure managements. Improved simplicity and batch fabrication of these hybrid printing techniques would provide a route for high-volume production of low-cost devices for disseminating the products and services even to rural areas. Given these collective considerations and their clinical importance, the research field of the human skin and eye-interfaced health monitoring systems remains critical to drive further innovations and widespread clinical adoption.

Conflict of Interest

The authors declare no conflict of interest.

[1] Y. Yang, W. Gao, *Chem. Soc. Rev.* **2019**, *48*, 1465.
[2] W. Gao, S. Emaminejad, H. Y. Y. Nyein, S. Challa, K. Chen, A. Peck, H. M. Fahad, H. Ota, H. Shiraki, D. Kiriya, D.-H. Lien, G. A. Brooks, R. W. Davis, A. Javey, *Nature* **2016**, *529*, 509.

**ADVANCED
SCIENCE NEWS**

www.advancedsciencenews.com

**ADVANCED
MATERIALS**

www.advmat.de

[3] Z. Huang, Y. Hao, Y. Li, H. Hu, C. Wang, A. Nomoto, T. Pan, Y. Gu, Y. Chen, T. Zhang, W. Li, Y. Lei, N. Kim, C. Wang, L. Zhang, J. W. Ward, A. Maralani, X. Li, M. F. Durstock, A. Pisano, Y. Lin, S. Xu, *Nat. Electron.* **2018**, *1*, 473.

[4] Y. Khan, A. E. Ostfeld, C. M. Lochner, A. Pierre, A. C. Arias, *Adv. Mater.* **2016**, *28*, 4373.

[5] W. Gao, H. Ota, D. Kiriya, K. Takei, A. Javey, *Acc. Chem. Res.* **2019**, *52*, 523.

[6] Y. Jiang, X. Li, B. Liu, J. Yi, Y. Fang, F. Shi, X. Gao, E. Sudzilovsky, R. Parameswaran, K. Koehler, V. Nair, J. Yue, K. Guo, Y. Fang, H.-M. Tsai, G. Freyermuth, R. C. S. Wong, C.-M. Kao, C.-T. Chen, A. W. Nicholls, X. Wu, G. M. G. Shepherd, B. Tian, *Nat. Biomed. Eng.* **2018**, *2*, 508.

[7] H. Fang, K. J. Yu, C. Gloschat, Z. Yang, E. Song, C.-H. Chiang, J. Zhao, S. M. Won, S. Xu, M. Trumpis, Y. Zhong, S. W. Han, Y. Xue, D. Xu, S. W. Choi, G. Cauwenberghs, M. Kay, Y. Huang, J. Viventi, I. R. Efimov, J. A. Rogers, *Nat. Biomed. Eng.* **2017**, *1*, 0038.

[8] K. J. Seo, P. Artoni, Y. Qiang, Y. Zhong, X. Han, Z. Shi, W. Yao, M. Fagiolini, H. Fang, *Adv. Biosyst.* **2019**, *3*, 1800276.

[9] Y. Qiang, P. Artoni, K. J. Seo, S. Culaclii, V. Hogan, X. Zhao, Y. Zhong, X. Han, P.-M. Wang, Y.-K. Lo, Y. Li, H. A. Patel, Y. Huang, A. Sambangi, J. S. V. Chu, W. Liu, M. Fagiolini, H. Fang, *Sci. Adv.* **2018**, *4*, eaat0626.

[10] M. Y. Rotenberg, B. Tian, *Nat. Biomed. Eng.* **2017**, *1*, 0048.

[11] B. Xu, A. Akhtar, Y. Liu, H. Chen, W.-H Yeo, S. I. Park, B. Boyce, H. Kim, J. Yu, H.-Y. Lai, S. Jung, Y. Zhou, J. Kim, S. Cho, Y. Huang, T. Bretl, J. A. Rogers, *Adv. Mater.* **2016**, *28*, 4462.

[12] V. K. Samineni, J. Yoon, K. E. Crawford, Y. R. Jeong, K. C. McKenzie, G. Shin, Z. Xie, S. S. Sundaram, Y. Li, M. Y. Yang, J. Kim, D. Wu, Y. Xue, X. Feng, Y. Huang, A. D. Mickle, A. Banks, J. S. Ha, J. P. Golden, J. A. Rogers, R. W. Gereau, *Pain* **2017**, *158*, 2108.

[13] C. Wang, X. Li, H. Hu, L. Zhang, Z. Huang, M. Lin, Z. Zhang, Z. Yin, B. Huang, H. Gong, S. Bhaskaran, Y. Gu, M. Makihata, Y. Guo, Y. Lei, Y. Chen, C. Wang, Y. Li, T. Zhang, Z. Chen, A. P. Pisano, L. Zhang, Q. Zhou, S. Xu, *Nat. Biomed. Eng.* **2018**, *2*, 687.

[14] A. J. Bandodkar, P. Gutruf, J. Choi, K. Lee, Y. Sekine, J. T. Reeder, W. J. Jeang, A. J. Aranyosi, S. P. Lee, J. B. Model, R. Ghaffari, C.-J. Su, J. P. Leshock, T. Ray, A. Verrillo, K. Thomas, V. Krishnamurthi, S. Han, J. Kim, S. Krishnan, T. Hang, J. A. Rogers, *Sci. Adv.* **2019**, *5*, eaav3294.

[15] S. Han, J. Kim, S. M. Won, Y. Ma, D. Kang, Z. Xie, K.-T. Lee, H. U. Chung, A. Banks, S. Min, S. Y. Heo, C. R. Davies, J. W. Lee, C.-H. Lee, B. H. Kim, K. Li, Y. Zhou, C. Wei, X. Feng, Y. Huang, J. A. Rogers, *Sci. Transl. Med.* **2018**, *10*, eaan4950.

[16] S. Y. Heo, J. Kim, P. Gutruf, A. Banks, P. Wei, R. Pielak, G. Balooch, Y. Shi, H. Araki, D. Rollo, C. Gaede, M. Patel, J. W. Kwak, A. E. Peña-Alcántara, K.-T. Lee, Y. Yun, J. K. Robinson, S. Xu, J. A. Rogers, *Sci. Transl. Med.* **2018**, *10*, eaau1643.

[17] H. U. Chung, B. H. Kim, J. Y. Lee, J. Lee, Z. Xie, E. M. Ibler, K. Lee, A. Banks, J. Y. Jeong, J. Kim, C. Ogle, D. Grande, Y. Yu, H. Jang, P. Assem, D. Ryu, J. W. Kwak, M. Namkoong, J. B. Park, Y. Lee, D. H. Kim, A. Ryu, J. Jeong, K. You, B. Ji, Z. Liu, Q. Huo, X. Feng, Y. Deng, Y. Xu, K.-I. Jang, J. Kim, Y. Zhang, R. Ghaffari, C. M. Rand, M. Schau, A. Hamvas, D. E. Weese-Mayer, Y. Huang, S. M. Lee, C. H. Lee, N. R. Shanbhag, A. S. Paller, S. Xu, J. A. Rogers, *Science* **2019**, *363*, eaau0780.

[18] J. T. Reeder, J. Choi, Y. Xue, P. Gutruf, J. Hanson, M. Liu, T. Ray, A. J. Bandodkar, R. Avila, W. Xia, S. Krishnan, S. Xu, K. Barnes, M. Pahnke, R. Ghaffari, Y. Huang, J. A. Rogers, *Sci. Adv.* **2019**, *5*, eaau6356.

[19] S. P. Lee, G. Ha, D. E. Wright, Y. Ma, E. Sen-Gupta, N. R. Haubrich, P. C. Branche, W. Li, G. L. Huppert, M. Johnson, H. B. Mutlu, K. Li, N. Sheth, J. A. Wright, Y. Huang, M. Mansour, J. A. Rogers, R. Ghaffari, *npj Digital Med.* **2018**, *1*, 2.

[20] X. Chen, Y. J. Park, M. Kang, S.-K. Kang, J. Koo, S. M. Shinde, J. Shin, S. Jeon, G. Park, Y. Yan, M. R. MacEwan, W. Z. Ray, K.-M. Lee, J. A. Rogers, J.-H. Ahn, *Nat. Commun.* **2018**, *9*, 1690.

[21] K.-I. Jang, K. Li, H. U. Chung, S. Xu, H. N. Jung, Y. Yang, J. W. Kwak, H. H. Jung, J. Song, C. Yang, A. Wang, Z. Liu, J. Y. Lee, B. H. Kim, J.-H. Kim, J. Lee, Y. Yu, B. J. Kim, H. Jang, K. J. Yu, J. Kim, J. W. Lee, J.-W. Jeong, Y. M. Song, Y. Huang, Y. Zhang, J. A. Rogers, *Nat. Commun.* **2017**, *8*, 15894.

[22] A. J. Bandodkar, J.-M. You, N.-H. Kim, Y. Gu, R. Kumar, A. M. V. Mohan, J. Kurniawan, S. Imani, T. Nakagawa, B. Parish, M. Parthasarathy, P. P. Mercier, S. Xu, J. Wang, *Energy Environ. Sci.* **2017**, *10*, 1581.

[23] Y. Lee, J. Kim, H. Joo, M. S. Raj, R. Ghaffari, D.-H. Kim, *Adv. Mater. Technol.* **2017**, *2*, 1700053.

[24] M. Bariya, Z. Shahpar, H. Park, J. Sun, Y. Jung, W. Gao, H. Y. Y. Nyein, T. S. Liaw, L.-C. Tai, Q. P. Ngo, M. Chao, Y. Zhao, M. Hettick, G. Cho, A. Javey, *ACS Nano* **2018**, *12*, 6978.

[25] S. Imani, A. J. Bandodkar, A. M. V. Mohan, R. Kumar, S. Yu, J. Wang, P. P. Mercier, *Nat. Commun.* **2016**, *7*, 11650.

[26] S.-Z. Guo, K. Qiu, F. Meng, S. H. Park, M. C. McAlpine, *Adv. Mater.* **2017**, *29*, 1701218.

[27] H. Ota, S. Emaminejad, Y. Gao, A. Zhao, E. Wu, S. Challa, K. Chen, H. M. Fahad, A. K. Jha, D. Kiriya, W. Gao, H. Shiraki, K. Morioka, A. R. Ferguson, K. E. Healy, R. W. Davis, A. Javey, *Adv. Mater. Technol.* **2016**, *1*, 1600013.

[28] J. T. Muth, D. M. Vogt, R. L. Truby, Y. Mengüç, D. B. Kolesky, R. J. Wood, J. A. Lewis, *Adv. Mater.* **2014**, *26*, 6307.

[29] A. D. Valentine, T. A. Busbee, J. W. Boley, J. R. Raney, A. Chortos, A. Kotikian, J. D. Berrigan, M. F. Durstock, J. A. Lewis, *Adv. Mater.* **2017**, *29*, 1703817.

[30] J. Kim, M. Kim, M.-S. Lee, K. Kim, S. Ji, Y.-T. Kim, J. Park, K. Na, K.-H. Bae, H. Kyun Kim, F. Bien, C. Young Lee, J.-U. Park, *Nat. Commun.* **2017**, *8*, 14997.

[31] J. Park, J. Kim, S.-Y. Kim, W. H. Cheong, J. Jang, Y.-G. Park, K. Na, Y.-T. Kim, J. H. Heo, C. Y. Lee, J. H. Lee, F. Bien, J.-U. Park, *Sci. Adv.* **2018**, *4*, eaap9841.

[32] K. Qiu, Z. Zhao, G. Haghiashtiani, S.-Z. Guo, M. He, R. Su, Z. Zhu, D. B. Bhuiyan, P. Murugan, F. Meng, S. H. Park, C.-C. Chu, B. M. Ogle, D. A. Saltzman, B. R. Konety, R. M. Sweet, M. C. McAlpine, *Adv. Mater. Technol.* **2018**, *3*, 1700235.

[33] J. Kim, G. A. Salvatore, H. Araki, A. M. Chiarelli, Z. Xie, A. Banks, X. Sheng, Y. Liu, J. W. Lee, K.-I. Jang, S. Y. Heo, K. Cho, H. Luo, B. Zimmerman, J. Kim, L. Yan, X. Feng, S. Xu, M. Fabiani, G. Gratton, Y. Huang, U. Paik, J. A. Rogers, *Sci. Adv.* **2016**, *2*, e1600418.

[34] S. Xu, Y. Zhang, L. Jia, K. E. Mathewson, K.-I. Jang, J. Kim, H. Fu, X. Huang, P. Chava, R. Wang, S. Bhole, L. Wang, Y. J. Na, Y. Guan, M. Flavin, Z. Han, Y. Huang, J. A. Rogers, *Science* **2014**, *344*, 70.

[35] M. S. Mannoor, Z. Jiang, T. James, Y. L. Kong, K. A. Malatesta, W. O. Soboyejo, N. Verma, D. H. Gracias, M. C. McAlpine, *Nano Lett.* **2013**, *13*, 2634.

[36] L. A. Hockaday, K. H. Kang, N. W. Colangelo, P. Y. C. Cheung, B. Duan, E. Malone, J. Wu, L. N. Girardi, L. J. Bonassar, H. Lipson, C. C. Chu, J. T. Butcher, *Biofabrication* **2012**, *4*, 035005.

[37] M. A. Meitl, Z.-T. Zhu, V. Kumar, K. J. Lee, X. Feng, Y. Y. Huang, I. Adesida, R. G. Nuzzo, J. A. Rogers, *Nat. Mater.* **2006**, *5*, 33.

[38] Z. Yan, T. Pan, M. Xue, C. Chen, Y. Cui, G. Yao, L. Huang, F. Liao, W. Jing, H. Zhang, M. Gao, D. Guo, Y. Xia, Y. Lin, *Adv. Sci.* **2017**, *4*, 1700251.

[39] D. S. Wie, Y. Zhang, M. K. Kim, B. Kim, S. Park, Y.-J. Kim, P. P. Irazoqui, X. Zheng, B. Xu, C. H. Lee, *Proc. Natl. Acad. Sci. USA* **2018**, *115*, E7236.

[40] B. H. Lee, Y. H. Cho, H. Lee, K. D. Lee, S. H. Kim, M. M. Sung, *Adv. Mater.* **2007**, *19*, 1714.

ADVANCED
SCIENCE NEWS

www.advancedsciencenews.com

ADVANCED
MATERIALS

www.advmat.de

[41] S. Kim, J. Wu, A. Carlson, S. H. Jin, A. Kovalsky, P. Glass, Z. Liu, N. Ahmed, S. L. Elgan, W. Chen, P. M. Ferreira, M. Sitti, Y. Huang, J. A. Rogers, *Proc. Natl. Acad. Sci. USA* **2010**, *107*, 17095.

[42] A. Carlson, H.-J. Kim-Lee, J. Wu, P. Elvikis, H. Cheng, A. Kovalsky, S. Elgan, Q. Yu, P. M. Ferreira, Y. Huang, K. T. Turner, J. A. Rogers, *Appl. Phys. Lett.* **2011**, *98*, 264104.

[43] A. A. M. Al-Okaily, J. A. Rogers, P. M. Ferreira, *J. Micro Nanomanuf.* **2014**, *2*, 011002.

[44] M. K. Choi, J. Yang, K. Kang, D. C. Kim, C. Choi, C. Park, S. J. Kim, S. I. Chae, T.-H. Kim, J. H. Kim, T. Hyeon, D.-H. Kim, *Nat. Commun.* **2015**, *6*, 7149.

[45] C. Linghu, C. Wang, N. Cen, J. Wu, Z. Lai, J. Song, *Soft Matter* **2019**, *15*, 30.

[46] J. D. Eisenhaure, S. I. Rhee, A. M. Al-Okaily, A. Carlson, P. M. Ferreira, S. Kim, *J. Microelectromech. Syst.* **2014**, *23*, 1012.

[47] X. Feng, M. A. Meitl, A. M. Bowen, Y. Huang, R. G. Nuzzo, J. A. Rogers, *Langmuir* **2007**, *23*, 12555.

[48] X. Ma, Q. Liu, D. Xu, Y. Zhu, S. Kim, Y. Cui, L. Zhong, M. Liu, *Nano Lett.* **2017**, *16*, 33.

[49] S. W. Bedell, D. Shahrjerdi, B. Hekmatshoar, K. Fogel, P. A. Lauro, J. A. Ott, N. Sosa, D. Sadana, *IEEE J. Photovoltaics* **2012**, *2*, 141.

[50] D. Shahrjerdi, S. W. Bedell, C. Bayram, C. C. Lubguban, K. Fogel, P. Lauro, J. A. Ott, M. Hopstaken, M. Gayness, D. Sadana, *Adv. Energy Mater.* **2013**, *3*, 566.

[51] Y. Zhang, Q. Liu, B. Xu, *Extreme Mech. Lett.* **2017**, *16*, 33.

[52] C. H. Lee, D. R. Kim, X. Zheng, *Nano Lett.* **2011**, *11*, 3435.

[53] E. Menard, K. J. Lee, D. Y. Khang, R. G. Nuzzo, J. A. Rogers, *Appl. Phys. Lett.* **2004**, *84*, 5398.

[54] Y. Sun, J. A. Rogers, *Adv. Mater.* **2007**, *19*, 1897.

[55] A. J. Baca, J.-H. Ahn, Y. Sun, M. A. Meitl, E. Menard, H.-S. Kim, W. M. Choi, D.-H. Kim, Y. Huang, J. A. Rogers, *Angew. Chem., Int. Ed.* **2008**, *47*, 5524.

[56] Y. Sun, S. Kim, I. Adesida, J. A. Rogers, *Appl. Phys. Lett.* **2005**, *87*, 083501.

[57] S.-I. Park, Y. Xiong, R.-H. Kim, P. Elvikis, M. Meitl, D.-H. Kim, J. Wu, J. Yoon, C.-J. Yu, Z. Liu, Y. Huang, K.-c. Hwang, P. Ferreira, X. Li, K. Choquette, J. A. Rogers, *Science* **2009**, *325*, 977.

[58] Y. Sun, D. Y. Khang, F. Hua, K. Hurley, R. G. Nuzzo, J. A. Rogers, *Adv. Funct. Mater.* **2005**, *15*, 30.

[59] Y. Sun, J. A. Rogers, *Nano Lett.* **2004**, *4*, 1953.

[60] Y. Sun, R. A. Graff, M. S. Strano, J. A. Rogers, *Small* **2005**, *1*, 1052.

[61] T.-H. Kim, K.-S. Cho, E. K. Lee, S. J. Lee, J. Chae, J. W. Kim, D. H. Kim, J.-Y. Kwon, G. Amaratunga, S. Y. Lee, B. L. Choi, Y. Kuk, J. M. Kim, K. Kim, *Nat. Photonics* **2011**, *5*, 176.

[62] K. Hoshino, T. C. Turner, S. Kim, A. Gopal, X. Zhang, *Langmuir* **2008**, *24*, 13804.

[63] A. Rizzo, M. Mazzeo, M. Palumbo, G. Lerario, S. D'Amone, R. Cingolani, G. Gigli, *Adv. Mater.* **2008**, *20*, 1886.

[64] A. Javey, Nam, R. S. Friedman, H. Yan, C. M. Lieber, *Nano Lett.* **2007**, *7*, 773.

[65] C. H. Lee, D. R. Kim, X. Zheng, *Proc. Natl. Acad. Sci. USA* **2010**, *107*, 9950.

[66] S. Nam, X. Jiang, Q. Xiong, D. Ham, C. M. Lieber, *Proc. Natl. Acad. Sci. USA* **2009**, *106*, 21035.

[67] A. J. Baca, K. J. Yu, J. Xiao, S. Wang, J. Yoon, J. H. Ryu, D. Stevenson, R. G. Nuzzo, A. A. Rockett, Y. Huang, J. A. Rogers, *Energy Environ. Sci.* **2010**, *3*, 208.

[68] Y. Yang, Y. Hwang, H. A. Cho, J.-H. Song, S.-J. Park, J. A. Rogers, H. C. Ko, *Small* **2011**, *7*, 484.

[69] S. Lee, B. Kang, H. Keum, N. Ahmed, J. A. Rogers, P. M. Ferreira, S. Kim, B. Min, *Sci. Rep.* **2016**, *6*, 27621.

[70] S. Xu, Z. Yan, K.-I. Jang, W. Huang, H. Fu, J. Kim, Z. Wei, M. Flavin, J. McCracken, R. Wang, A. Badea, Y. Liu, D. Xiao, G. Zhou, J. Lee, H. U. Chung, H. Cheng, W. Ren, A. Banks, X. Li,

U. Paik, R. G. Nuzzo, Y. Huang, Y. Zhang, J. A. Rogers, *Science* **2015**, *347*, 154.

[71] Z. Yan, F. Zhang, F. Liu, M. Han, D. Ou, Y. Liu, Q. Lin, X. Guo, H. Fu, Z. Xie, M. Gao, Y. Huang, J. Kim, Y. Qiu, K. Nan, J. Kim, P. Gutruf, H. Luo, A. Zhao, K.-C. Hwang, Y. Huang, Y. Zhang, J. A. Rogers, *Sci. Adv.* **2016**, *2*, e1601014.

[72] Y. Zhang, Z. Yan, K. Nan, D. Xiao, Y. Liu, H. Luan, H. Fu, X. Wang, Q. Yang, J. Wang, W. Ren, H. Si, F. Liu, L. Yang, H. Li, J. Wang, X. Guo, H. Luo, L. Wang, Y. Huang, J. A. Rogers, *Proc. Natl. Acad. Sci. USA* **2015**, *112*, 11757.

[73] Z. Yan, F. Zhang, J. Wang, F. Liu, X. Guo, K. Nan, Q. Lin, M. Gao, D. Xiao, Y. Shi, Y. Qiu, H. Luan, J. H. Kim, Y. Wang, H. Luo, M. Han, Y. Huang, Y. Zhang, J. A. Rogers, *Adv. Funct. Mater.* **2016**, *26*, 2629.

[74] J. W. Hutchinson, Z. Suo, *Adv. Appl. Mech.* **1991**, *29*, 63.

[75] A. N. Gent, S. M. Lai, *J. Polym. Sci., Part B: Polym. Phys.* **1994**, *32*, 1543.

[76] N. A. Melosh, A. Boukai, F. Diana, B. Gerardot, A. Badolato, P. M. Petroff, J. R. Heath, *Science* **2003**, *300*, 112.

[77] R. Saeidpourazar, R. Li, Y. Li, M. D. Sangid, C. Lu, Y. Huang, J. A. Rogers, P. M. Ferreira, *J. Microelectromech. Syst.* **2012**, *21*, 1049.

[78] H. Yi, M. Seong, K. Sun, I. Hwang, K. Lee, C. Cha, T.-i. Kim, H. E. Jeong, *Adv. Funct. Mater.* **2018**, *28*, 1706498.

[79] A. Jong-Hyun, K. Hoon-Sik, L. Keon Jae, Z. Zhengtao, E. Menard, R. G. Nuzzo, J. A. Rogers, *IEEE Electron Device Lett.* **2006**, *27*, 460.

[80] A. Alharbi, B. Nasri, T. Wu, D. Shahrjerdi, in *2016 IEEE Int. Electron Devices Meeting (IEDM)*, IEEE, Piscataway, NJ, USA **2016**, p. 6.5.1.

[81] S. W. Bedell, K. Fogel, P. Lauro, D. Shahrjerdi, J. A. Ott, D. Sadana, *J. Phys. D: Appl. Phys.* **2013**, *46*, 152002.

[82] F. Dross, J. Robbelein, B. Vandevelde, E. Van Kerschaver, I. Gordon, G. Beaucarne, J. Poortmans, *Appl. Phys. A* **2007**, *89*, 149.

[83] C. H. Lee, D. R. Kim, X. Zheng, *ACS Nano* **2014**, *8*, 8746.

[84] D. Shahrjerdi, S. W. Bedell, *Nano Lett.* **2013**, *13*, 315.

[85] G.-T. Hwang, H. Park, J.-H. Lee, S. Oh, K.-I. Park, M. Byun, H. Park, G. Ahn, C. K. Jeong, K. No, H. Kwon, S.-G. Lee, B. Joung, K. J. Lee, *Adv. Mater.* **2014**, *26*, 4880.

[86] C. H. Lee, D. R. Kim, I. S. Cho, N. William, Q. Wang, X. Zheng, *Sci. Rep.* **2012**, *2*, 1000.

[87] C. H. Lee, J.-H. Kim, C. Zou, I. S. Cho, J. M. Weisse, W. Nemeth, Q. Wang, A. C. T. van Duin, T.-S. Kim, X. Zheng, *Sci. Rep.* **2013**, *3*, 2917.

[88] F. M. Fowkes, *J. Phys. Chem.* **1963**, *67*, 2538.

[89] D. H. Park, H. W. Park, J. W. Chung, K. Nam, S. Choi, Y. S. Chung, H. Hwang, B. Kim, D. H. Kim, *Adv. Funct. Mater.* **2019**, *29*, 1808909.

[90] B. Y. Ahn, E. B. Duoss, M. J. Motala, X. Guo, S.-I. Park, Y. Xiong, J. Yoon, R. G. Nuzzo, J. A. Rogers, J. A. Lewis, *Science* **2009**, *323*, 1590.

[91] W. Lee, Y. Liu, Y. Lee, B. K. Sharma, S. M. Shinde, S. D. Kim, K. Nan, Z. Yan, M. Han, Y. Huang, Y. Zhang, J.-H. Ahn, J. A. Rogers, *Nat. Commun.* **2018**, *9*, 1417.

[92] J. S. Park, T. Kim, W. S. Kim, *Sci. Rep.* **2017**, *7*, 3246.

[93] J. U. Lind, T. A. Busbee, A. D. Valentine, F. S. Pasqualini, H. Yuan, M. Yadid, S.-J. Park, A. Kotikian, A. P. Nesmith, P. H. Campbell, J. J. Vlassak, J. A. Lewis, K. K. Parker, *Nat. Mater.* **2017**, *16*, 303.

[94] B. Chen, Y. Jiang, X. Tang, Y. Pan, S. Hu, *ACS Appl. Mater. Interfaces* **2017**, *9*, 28433.

[95] E. B. Secor, B. Y. Ahn, T. Z. Gao, J. A. Lewis, M. C. Hersam, *Adv. Mater.* **2015**, *27*, 6683.

[96] Z. Zhu, S.-Z. Guo, T. Hirdler, C. Eide, X. Fan, J. Tolar, M. C. McAlpine, *Adv. Mater.* **2018**, *30*, 1707495.

[97] W. H. Herschel, R. Bulkley, *Kolloid-Z.* **1926**, *39*, 291.

[98] J. A. Lewis, *Adv. Funct. Mater.* **2006**, *16*, 2193.

[99] A. Sydney Gladman, E. A. Matsumoto, R. G. Nuzzo, L. Mahadevan, J. A. Lewis, *Nat. Mater.* **2016**, *15*, 413.

[100] A. E. Jakus, E. B. Secor, A. L. Rutz, S. W. Jordan, M. C. Hersam, R. N. Shah, *ACS Nano* **2015**, *9*, 4636.

[101] Z. Derafshi, B. E. Kunzer, E. M. Mugler, N. Rokhmanova, D.-W. Park, H. Tajalli, K. Shetty, Z. Ma, J. C. Williams, J. R. Hetling, *Invest. Opthalmol. Visual Sci.* **2017**, *58*, 2863.

[102] R. A. Smith, V. Cokkinides, H. J. Eyre, *Ca-Cancer J. Clin.* **2003**, *53*, 27.

[103] M. Bariya, H. Y. Y. Nyein, A. Javey, *Nat. Electron.* **2018**, *1*, 160.

[104] M. K. Choi, I. Park, D. C. Kim, E. Joh, O. K. Park, J. Kim, M. Kim, C. Choi, J. Yang, K. W. Cho, J.-H. Hwang, J.-M. Nam, T. Hyeon, J. H. Kim, D.-H. Kim, *Adv. Funct. Mater.* **2015**, *25*, 7109.

[105] J. Kim, A. Banks, H. Cheng, Z. Xie, S. Xu, K.-I. Jang, J. W. Lee, Z. Liu, P. Gutruf, X. Huang, P. Wei, F. Liu, K. Li, M. Dalal, R. Ghaffari, X. Feng, Y. Huang, S. Gupta, U. Paik, J. A. Rogers, *Small* **2015**, *11*, 906.

[106] W.-H. Yeo, Y.-S. Kim, J. Lee, A. Ameen, L. Shi, M. Li, S. Wang, R. Ma, S. H. Jin, Z. Kang, Y. Huang, J. A. Rogers, *Adv. Mater.* **2013**, *25*, 2773.

[107] S. Biagi, S. Ghimenti, M. Onor, E. Bramanti, *Biomed. Chromatogr.* **2012**, *26*, 1408.

[108] J. Moyer, D. Wilson, I. Finkelshtein, B. Wong, R. Potts, *Diabetes Technol. Ther.* **2012**, *14*, 398.

[109] W. Jia, A. J. Bandodkar, G. Valdés-Ramírez, J. R. Windmiller, Z. Yang, J. Ramírez, G. Chan, J. Wang, *Anal. Chem.* **2013**, *85*, 6553.

[110] A. Martín, J. Kim, J. F. Kurniawan, J. R. Sempionatto, J. R. Moreto, G. Tang, A. S. Campbell, A. Shin, M. Y. Lee, X. Liu, J. Wang, *ACS Sens.* **2017**, *2*, 1860.

[111] A. Abellán-Llobregat, I. Jeerapan, A. Bandodkar, L. Vidal, A. Canals, J. Wang, E. Morallón, *Biosens. Bioelectron.* **2017**, *91*, 885.

[112] H. Lee, T. K. Choi, Y. B. Lee, H. R. Cho, R. Ghaffari, L. Wang, H. J. Choi, T. D. Chung, N. Lu, T. Hyeon, S. H. Choi, D.-H. Kim, *Nat. Nanotechnol.* **2016**, *11*, 566.

[113] S. Y. Oh, S. Y. Hong, Y. R. Jeong, J. Yun, H. Park, S. W. Jin, G. Lee, J. H. Oh, H. Lee, S.-S. Lee, J. S. Ha, *ACS Appl. Mater. Interfaces* **2018**, *10*, 13729.

[114] M. J. Joyner, *Exercise Sport Sci. Rev.* **2001**, *29*, 139.

[115] S. Wang, G. Zhang, H. Meng, L. Li, *Skin Res. Technol.* **2013**, *19*, e312.

[116] S. F. Godek, A. R. Bartolozzi, J. J. Godek, *Br. J. Sports Med.* **2005**, *39*, 205.

[117] S. Emaminejad, W. Gao, E. Wu, Z. A. Davies, H. Yin Yin Nyein, S. Challa, S. P. Ryan, H. M. Fahad, K. Chen, Z. Shahpar, S. Talebi, C. Milla, A. Javey, R. W. Davis, *Proc. Natl. Acad. Sci. USA* **2017**, *114*, 4625.

[118] J. Heikenfeld, *Electroanalysis* **2016**, *28*, 1242.

[119] P. Salvo, F. D. Francesco, D. Costanzo, C. Ferrari, M. G. Trivella, D. D. Rossi, *IEEE Sens. J.* **2010**, *10*, 1557.

[120] S. Jadoon, S. Karim, M. R. Akram, A. Kalsoom Khan, M. A. Zia, A. R. Siddiqi, G. Murtaza, *Int. J. Anal. Chem.* **2015**, *2015*, 1.

[121] A. Mishra, R. Greaves, J. Massie, *Clin. Biochem. Rev.* **2005**, *26*, 135.

[122] Y. Y. Al-Tamer, E. A. Hadi, I. E. I. Al-Badrani, *Urol. Res.* **1997**, *25*, 337.

[123] G. Yosipovitch, J. Reis, E. Tur, E. Sprecher, D. Yarnitsky, G. Boner, *Br. J. Dermatol.* **1995**, *133*, 561.

[124] J. Gonzalo-Ruiz, R. Mas, C. de Haro, E. Cabruja, R. Camero, M. A. Alonso-Lomillo, F. J. Muñoz, *Biosens. Bioelectron.* **2009**, *24*, 1788.

[125] S. M. Abbott, K. J. Reid, P. C. Zee, *Psychiatr. Clin. North Am.* **2015**, *38*, 805.

[126] H. J. Burgess, J. S. Emens, *Curr. Sleep Med. Rep.* **2016**, *2*, 158.

[127] M. A. Carskadon, S. E. Labyak, C. Acebo, R. Seifer, *Neurosci. Lett.* **1999**, *260*, 129.

[128] R. M. Allman, P. S. Goode, N. Burst, A. A. Bartolucci, D. R. Thomas, *Adv. Wound Care* **1999**, *12*, 22.

[129] J. D. Whitney, *J. Wound Ostomy Continence Nurs.* **2000**, *27*, 293.

[130] C. H. Lyder, Y. Wang, M. Metersky, M. Curry, R. Kliman, N. R. Verzier, D. R. Hunt, *J. Am. Geriatr. Soc.* **2012**, *60*, 1603.

[131] D. Dijk, C. Czeisler, *J. Neurosci.* **1995**, *15*, 3526.

[132] J. A. Sarabia, M. A. Rol, P. Mendiola, J. A. Madrid, *Physiol. Behav.* **2008**, *95*, 570.

[133] W. Harrison, D. Goodman, *JAMA Pediatr.* **2015**, *169*, 855.

[134] J. M. Fanaroff, A. A. Fanaroff, *Semin. Fetal Neonat. Med.* **2006**, *11*, 174.

[135] L. A. Smith, P. J. Dawes, B. C. Galland, *Sleep Med. Rev.* **2018**, *37*, 4.

[136] P. H. T. Cartlidge, P. E. Fox, N. Rutter, *Early Hum. Dev.* **1990**, *21*, 1.

[137] A. C. Tottman, J. M. Alsweiler, F. H. Bloomfield, J. E. Harding, *Arch. Dis. Child. - Fetal Neonat. Ed.* **2018**, *103*, F277.

[138] C. Lund, *Newborn Infant Nurs. Rev.* **2014**, *14*, 160.

[139] S. Bouwstra, W. Chen, L. Feijs, S. B. Oetomo, in *2009 Sixth Int. Workshop on Wearable and Implantable Body Sensor Networks*, IEEE, Piscataway, NJ, USA **2009**, p. 162.

[140] K. Wright, *J. Wound Ostomy Continence Nurs.* **2004**, *31*, 315.

[141] D.-H. Kim, N. Lu, R. Ma, Y.-S. Kim, R.-H. Kim, S. Wang, J. Wu, S. M. Won, H. Tao, A. Islam, K. J. Yu, T.-I. Kim, R. Chowdhury, M. Ying, L. Xu, M. Li, H.-J. Chung, H. Keum, M. McCormick, P. Liu, Y.-W. Zhang, F. G. Omenetto, Y. Huang, T. Coleman, J. A. Rogers, *Science* **2011**, *333*, 838.

[142] J. A. Fan, W.-H. Yeo, Y. Su, Y. Hattori, W. Lee, S.-Y. Jung, Y. Zhang, Z. Liu, H. Cheng, L. Falgout, M. Bajema, T. Coleman, D. Gregoire, R. J. Larsen, Y. Huang, J. A. Rogers, *Nat. Commun.* **2014**, *5*, 3266.

[143] Y. J. Hong, H. Lee, J. Kim, M. Lee, H. J. Choi, T. Hyeon, D.-H. Kim, *Adv. Funct. Mater.* **2018**, *28*, 1805754.

[144] E. A. Pelaez, E. R. Villegas, *Conf. Proc. IEEE Eng. Med. Biol. Soc.* IEEE, Lyon, France **2007**, 2296.

[145] Y. Ma, M. Pharr, L. Wang, J. Kim, Y. Liu, Y. Xue, R. Ning, X. Wang, H. U. Chung, X. Feng, J. A. Rogers, Y. Huang, *Small* **2017**, *13*, 1602954.

[146] L. Sinclair, J. Crisp, J. Sinn, *J. Paediatr. Child Health* **2009**, *45*, 535.

[147] L. A. Geddes, M. H. Voelz, C. F. Babbs, J. D. Bourland, W. A. Tacker, *Psychophysiology* **1981**, *18*, 71.

[148] J. S. Kim, Y. J. Chee, J. W. Park, J. W. Choi, K. S. Park, *Physiol. Meas.* **2006**, *27*, 203.

[149] A. J. Bandodkar, J. Wang, *Trends Biotechnol.* **2014**, *32*, 363.

[150] H. Lee, Y. J. Hong, S. Baik, T. Hyeon, D.-H. Kim, *Adv. Healthcare Mater.* **2018**, *7*, 1701150.

[151] É. Csősz, P. Boross, A. Csutak, A. Berta, F. Tóth, S. Póliska, Z. Török, J. Tőzsér, *J. Proteomics* **2012**, *75*, 2196.

[152] N. M. Farandos, A. K. Yetisen, M. J. Monteiro, C. R. Lowe, S. H. Yun, *Adv. Healthcare Mater.* **2015**, *4*, 792.

[153] M. Elsherif, M. U. Hassan, A. K. Yetisen, H. Butt, *ACS Nano* **2018**, *12*, 5452.

[154] J.-C. Chiou, S.-H. Hsu, Y.-C. Huang, G.-T. Yeh, W.-T. Liou, C.-K. Kuei, *Sensors* **2017**, *17*, 108.

[155] M. X. Chu, K. Miyajima, D. Takahashi, T. Arakawa, K. Sano, S.-i. Sawada, H. Kudo, Y. Iwasaki, K. Akiyoshi, M. Mochizuki, K. Mitsubayashi, *Talanta* **2011**, *83*, 960.

[156] Y.-T. Liao, H. Yao, A. Lingley, B. A. Parviz, B. P. Otis, *IEEE J. Solid-State Circuits* **2012**, *47*, 335.

[157] H. Yao, A. J. Shum, M. Cowan, I. Lähdesmäki, B. A. Parviz, *Biosens. Bioelectron.* **2011**, *26*, 3290.

[158] N. Thomas, I. Lähdesmäki, B. A. Parviz, *Sens. Actuators, B* **2012**, *162*, 128.

[159] M. Leonardi, E. M. Pitchon, A. Bertsch, P. Renaud, A. Mermoud, *Acta Ophthalmol.* **2009**, *87*, 433.

[160] P. Chen, S. Saati, R. Varma, M. S. Humayun, Y. Tai, *J. Microelectromech. Syst.* **2010**, *19*, 721.

[161] G.-Z. Chen, I.-S. Chan, D. C. C. Lam, *Sens. Actuators, A* **2013**, *203*, 112.

[162] R. Yin, Z. Xu, M. Mei, Z. Chen, K. Wang, Y. Liu, T. Tang, M. K. Priydarshi, X. Meng, S. Zhao, B. Deng, H. Peng, Z. Liu, X. Duan, *Nat. Commun.* **2018**, *9*, 2334.

[163] M. F. Marmor, A. B. Fulton, G. E. Holder, Y. Miyake, M. Brigell, M. Bach, *Doc. Ophthalmol.* **2009**, *118*, 69.

[164] K. Holopigian, W. Seiple, M. Lorenzo, R. Carr, *Invest. Ophthalmol. Visual Sci.* **1992**, *33*, 2773.

[165] E. Sundmark, *Acta Ophthalmol.* **1959**, *37*, 164.

[166] S. Viswanathan, L. J. Frishman, J. G. Robson, *Invest. Ophthalmol. Visual Sci.* **2000**, *41*, 2797.

[167] M. Gjötterberg, *Arch. Ophthalmol.* **1986**, *104*, 569.

[168] L. Esakowitz, A. Kriss, F. Shawkat, *Eye* **1993**, *7*, 169.

[169] F. Carpi, F. Tomei, *Biomed. Pharmacother.* **2006**, *60*, 375.

[170] N. Mohidin, M. K. H. Yap, R. J. Jacobs, *Sains Malays.* **2014**, *43*, 1089.

[171] J. Sun, Y. Chen, M. K. Priydarshi, Z. Chen, A. Bachmatiuk, Z. Zou, Z. Chen, X. Song, Y. Gao, M. H. Rümmeli, Y. Zhang, Z. Liu, *Nano Lett.* **2015**, *15*, 5846.

[172] X.-D. Chen, Z.-L. Chen, J.-Y. Sun, Y.-F. Zhang, Z.-F. Liu, *Acta Phys.-Chim. Sin.* **2016**, *32*, 14.

[173] J. Sun, Y. Zhang, Z. Liu, *ChemNanoMat* **2016**, *2*, 9.

[174] D. L. McCulloch, M. F. Marmor, M. G. Brigell, R. Hamilton, G. E. Holder, R. Tzekov, M. Bach, *Doc. Ophthalmol.* **2015**, *130*, 1.

[175] K. Mansouri, F. A. Medeiros, A. Tafreshi, R. N. Weinreb, *Arch. Ophthalmol.* **2012**, *130*, 1534.

[176] H. A. Quigley, A. T. Broman, *Brit. J. Ophthalmol.* **2006**, *90*, 262.

[177] M. Leonardi, P. Leuenberger, D. Bertrand, A. Bertsch, P. Renaud, *Invest. Opthalmol. Visual Sci.* **2004**, *45*, 3113.

[178] M. Detry, A. Boschi, G. Ellinghaus, J. F. De Plaen, *Eur. J. Ophthalmol.* **1996**, *6*, 273.

[179] H. A. Quigley, H. D. Jampel, *J. Glaucoma* **2003**, *12*, 451.

[180] American Diabetes Association, *Diabetes Care* **2014**, *37*, S81.

[181] Y. Liao, H. Yao, A. Lingley, B. Parviz, B. P. Otis, *IEEE J. Solid-State Circuits* **2012**, *47*, 335.

[182] J. Kim, A. S. Campbell, B. E.-F. de Ávila, J. Wang, *Nat. Biotechnol.* **2019**, *37*, 389.

[183] H. Yao, C. Marcheselli, A. Afanasiev, I. Lähdesmäki, B. A. Parviz, in *2012 IEEE 25th Int. Conf. on Micro Electro Mechanical Systems (MEMS)*, IEEE, Piscataway, NJ, USA **2012**, p. 769.

[184] I. M. Graz, D. P. J. Cotton, A. Robinson, S. P. Lacour, *Appl. Phys. Lett.* **2011**, *98*, 124101.

[185] A. Romeo, Q. Liu, Z. Suo, S. P. Lacour, *Appl. Phys. Lett.* **2013**, *102*, 131904.

[186] S. Ji, B. G. Hyun, K. Kim, S. Y. Lee, S.-H. Kim, J.-Y. Kim, M. H. Song, J.-U. Park, *NPG Asia Mater.* **2016**, *8*, e299.

[187] J. Wang, *Chem. Rev.* **2008**, *108*, 814.

[188] S. Singh, M. McShane, *Biosens. Bioelectron.* **2010**, *25*, 1075.

[189] D. K. Sen, G. S. Sarin, *Br. J. Ophthalmol.* **1980**, *64*, 693.

[190] P. Bollella, S. Sharma, A. E. G. Cass, R. Antiochia, *Biosens. Bioelectron.* **2019**, *123*, 152.

[191] A. M. V. Mohan, J. R. Windmiller, R. K. Mishra, J. Wang, *Biosens. Bioelectron.* **2017**, *91*, 574.

[192] R. K. Mishra, A. M. Vinu Mohan, F. Soto, R. Chrostowski, J. Wang, *Analyst* **2017**, *142*, 918.

[193] S. R. Corrie, J. W. Coffey, J. Islam, K. A. Markey, M. A. F. Kendall, *Analyst* **2015**, *140*, 4350.

[194] F. Lucarelli, F. Ricci, F. Caprio, F. Valgimigli, C. Scuffi, D. Moscone, G. Palleschi, *J. Diabetes Sci. Technol.* **2012**, *6*, 1172.

[195] W. Li, R. N. Terry, J. Tang, M. R. Feng, S. P. Schwendeman, M. R. Prausnitz, *Nat. Biomed. Eng.* **2019**, *3*, 220.

[196] C.-M. Horejs, *Nat. Rev. Mater.* **2019**, *4*, 80.

[197] B. Tian, J. Liu, T. Dvir, L. Jin, J. H. Tsui, Q. Qing, Z. Suo, R. Langer, D. S. Kohane, C. M. Lieber, *Nat. Mater.* **2012**, *11*, 986.

[198] G. Hong, T.-M. Fu, T. Zhou, T. G. Schuhmann, J. Huang, C. M. Lieber, *Nano Lett.* **2015**, *15*, 6979.

[199] J. Liu, T.-M. Fu, Z. Cheng, G. Hong, T. Zhou, L. Jin, M. Duvvuri, Z. Jiang, P. Kruskal, C. Xie, Z. Suo, Y. Fang, C. M. Lieber, *Nat. Nanotechnol.* **2015**, *10*, 629.

[200] T. G. Schuhmann, J. Yao, G. Hong, T.-M. Fu, C. M. Lieber, *Nano Lett.* **2017**, *17*, 5836.

[201] T.-M. Fu, G. Hong, R. D. Viveros, T. Zhou, C. M. Lieber, *Proc. Natl. Acad. Sci. USA* **2017**, *114*, E10046.

[202] G. Hong, T.-M. Fu, M. Qiao, R. D. Viveros, X. Yang, T. Zhou, J. M. Lee, H.-G. Park, J. R. Sanes, C. M. Lieber, *Science* **2018**, *360*, 1447.

[203] D. Weinstein, J. Leininger, C. Hamby, B. Safai, *J. Clin. Aesthetic Dermatol.* **2014**, *7*, 13.

[204] G. F. L. Hofbauer, J. Kamarashev, R. Geertsen, R. Böni, R. Dummer, *J. Cutaneous Pathol.* **1998**, *25*, 204.

[205] X. Jing, C. W. Michael, C. G. A. Theoharis, *Diagn. Cytopathol.* **2013**, *41*, 126.

[206] R. King, K. N. Weilbaecher, G. McGill, E. Cooley, M. Mihm, D. E. Fisher, *Am. J. Pathol.* **1999**, *155*, 731.

[207] M. Peng, Y. Wang, Q. Fu, F. Sun, N. Na, J. Ouyang, *Anal. Chem.* **2018**, *90*, 6206.

[208] H.-H. Hu, M. Guedj, V. Descamps, T. Jouary, A. Bourillon, K. Ezzedine, A. Taïeb, M. Bagot, A. Bensussan, P. Saiag, B. Grandchamp, N. Basset-Seguin, N. Soufir, *J. Dermatol. Sci.* **2011**, *64*, 127.

[209] X. Yan, H. Li, W. Zheng, X. Su, *Anal. Chem.* **2015**, *87*, 8904.

[210] B. Ciui, A. Martin, R. K. Mishra, B. Brunetti, T. Nakagawa, T. J. Dawkins, M. Lyu, C. Cristea, R. Sandulescu, J. Wang, *Adv. Healthcare Mater.* **2018**, *7*, 1701264.

[211] X. Dai, G. Hong, T. Gao, C. M. Lieber, *Acc. Chem. Res.* **2018**, *51*, 309.

[212] T.-M. Fu, G. Hong, T. Zhou, T. G. Schuhmann, R. D. Viveros, C. M. Lieber, *Nat. Methods* **2016**, *13*, 875.

[213] G. Hong, X. Yang, T. Zhou, C. M. Lieber, *Curr. Opin. Neurobiol.* **2018**, *50*, 33.

[214] L. R. Hochberg, D. Bacher, B. Jarosiewicz, N. Y. Masse, J. D. Simeral, J. Vogel, S. Haddadin, J. Liu, S. S. Cash, P. van der Smagt, J. P. Donoghue, *Nature* **2012**, *485*, 372.

[215] K. V. Shenoy, J. M. Carmena, *Neuron* **2014**, *84*, 665.

[216] V. S. Polikov, P. A. Tresco, W. M. Reichert, *J. Neurosci. Methods* **2005**, *148*, 1.

[217] J. A. Perge, M. L. Homer, W. Q. Malik, S. Cash, E. Eskandar, G. Friehs, J. P. Donoghue, L. R. Hochberg, *J. Neural Eng.* **2013**, *10*, 036004.

[218] R. Feiner, T. Dvir, *Nat. Rev. Mater.* **2017**, *3*, 17076.

[219] T. G. Schuhmann Jr., T. Zhou, G. Hong, J. M. Lee, T.-M. Fu, H.-G. Park, C. M. Lieber, *J. Vis. Exp.* **2018**, *137*, e58003.

[220] J. J. Jun, N. A. Steinmetz, J. H. Siegle, D. J. Denman, M. Bauza, B. Barbarits, A. K. Lee, C. A. Anastassiou, A. Andrei, Ç. Aydın, M. Barbic, T. J. Blanche, V. Bonin, J. Couto, B. Dutta, S. L. Gratiy, D. A. Gutnisky, M. Häusser, B. Karsh, P. Ledochowitsch, C. M. Lopez, C. Mitelut, S. Musa, M. Okun, M. Pachitariu, J. Putzeys, P. D. Rich, C. Rossant, W.-L. Sun, K. Svoboda, M. Carandini, K. D. Harris, C. Koch, J. O'Keefe, T. D. Harris, *Nature* **2017**, *551*, 232.

[221] A. Berényi, Z. Somogyvári, A. J. Nagy, L. Roux, J. D. Long, S. Fujisawa, E. Stark, A. Leonardo, T. D. Harris, G. Buzsáki, *J. Neurophysiol.* **2014**, *111*, 1132.

[222] T. A. LeGates, D. C. Fernandez, S. Hattar, *Nat. Rev. Neurosci.* **2014**, *15*, 443.

[223] K. S. Korshunov, L. J. Blakemore, P. Q. Trombley, *Front. Cell. Neurosci.* **2017**, *11*, 91.

[224] B.-H. Liu, A. D. Huberman, M. Scanziani, *Nature* **2016**, *538*, 383.

[225] D. E. Wilson, D. E. Whitney, B. Scholl, D. Fitzpatrick, *Nat. Neurosci.* **2016**, *19*, 1003.

[226] O. S. Dhande, A. D. Huberman, *Curr. Opin. Neurobiol.* **2014**, *24*, 133.

[227] S. Han, M. K. Kim, B. Wang, D. S. Wie, S. Wang, C. H. Lee, *Adv. Mater.* **2016**, *28*, 10257.